Energy Conversion and Management 203 (2020) 112180

Contents lists available at ScienceDirect

Energy Conversion and Management

journal homepage: www.elsevier.com/locate/enconman

# Studies on fast and green biodiesel production from an indigenous nonedible Indian feedstock using single phase strontium titanate catalyst

Shalini Sahani, Tania Roy, Yogesh Chandra Sharma*

*Department of Chemistry, Indian Institute of Technology (BHU) Varanasi, Varanasi 221005, India*

ARTICLE INFO

*Keywords:*
Transesterification
Perovskite
Response surface methodology
Box Behnkehn Design

ABSTRACT

Strontium titanate was synthesized by polymer precursor method and its catalytic activity as heterogeneous basic catalyst was tested in transesterification reaction for high-quality biodiesel production form *Madhuca indica* oil. The synthesized strontium titanate was characterized by powder X-ray Diffraction (XRD), X-Ray Photoelectron Spectroscopy (XPS), Field Emission Scanning Electron Microscopy (FESEM) attached with Energy Dispersive X-ray Spectroscopy (EDS), Transmission Electron Microscopy (TEM), Fourier Transform Infrared Spectroscopy (FTIR). Surface area and basicity were also determined using Brunauer-Emmett-Teller (BET) surface area analyzer and Hammett indicator method. The structural characterizations of catalyst enunciated the single perovskite phase formation of well-assorted strontium titanate nanospheres. The transesterification reaction was optimized using one variable at a time (OVAT) and Response Surface Methodology (RSM) using Box Behnkehn Design (BBD) to comprehend the linear effect and interactive effect of process variables on biodiesel production. The optimized reaction condition through OVAT was obtained as: catalyst dose (1.3 wt%), methanol to oil molar ratio (18:1), reaction temperature (65 °C), reaction time (120 min), and agitation speed (600 rpm) while RSM predicted the highest methyl ester conversion at optimum catalyst dose (1.19 wt%), methanol to oil molar ratio (21.5:1), reaction temperature (71 °C), and reaction time (97.7 min). The confirmatory experiment noticed the highest 98% FAME conversion at following reaction conditions catalyst dose (1.2 wt%), methanol to oil molar ratio (22:1), reaction temperature (65 °C), and reaction time (100 min). Confirmatory experiment showed its close agreement with the predicted values from RSM instead OVAT. According to RSM, catalyst dose, reaction temperature, reaction time, and methanol to oil molar ratio were influencing process parameters for transesterification in descending order of their strength. Furthermore, a pseudo-first-order kinetic model was established with the activation energy ($E_a$) of 65.95 kJ $mol^{-1}$. The Environmental Factor (E-factor) and Turn Over Frequency (TOF) were also determined and demonstrated the prepared catalyst as a sustainable and potential heterogeneous base catalyst. The physicochemical properties of produced biodiesel were evaluated to check its compatibility with conventional diesel fuel.

## 1. Introduction

Since energy requirement of global population of more than 8 billion present on earth has been drastically increased during last couple of decades, this compelled the research fraternity to explore the alternatives of existing exhaustible petroleum fuels which should be renewable and green energy resources [1]. So far, among all the explored renewable energy resources, biodiesel has found its versatile utilization in transport sector as most prominent renewable energy resource [2]. It is rapidly biodegradable in nature, carbon neutral and completely non toxic [3]. The combustion of biodiesel does not dump the harmful green house gases into atmosphere which makes it an appropriate substitute of conventional diesel. Moreover, biodiesel is widely prepared by an economically viable transesterification method also called as methanolysis when methanol is used in reaction [4]. This technique consumes vegetable oil as substrate and alcohol as reactant. Since this reaction is driven sluggishly without catalyst, a potential catalyst is required to carry out the reaction swiftly. Transesterification reaction requires either acid (sulfuric acid [5], hydrochloric acid [6], sulfonic acid [7], sulfated zirconia [8], sulfated tin oxide [8]) or base (KOH [9], NaOH [10], $BaZrO_3$ [11], BaO [12]) catalyst to drive out it in forward direction since it is a reversible reaction [2]. Many homogeneous and heterogeneous catalysts are explored for biodiesel production through transesterification. Eventually the application of heterogeneous catalyst

* Corresponding author.
*E-mail address:* ysharma.apc@itbhu.ac.in (Y.C. Sharma).

https://doi.org/10.1016/j.enconman.2019.112180
Received 18 July 2019; Received in revised form 10 October 2019; Accepted 11 October 2019
Available online 09 November 2019
0196-8904/ 

is quite preferable over homogeneous catalyst as former can find its reusability at large scale owing to easy solid–liquid separation from reaction mixture [13]. Moreover, heterogeneous acid catalyst are found to be lesser efficient than heterogeneous base catalyst as they catalyze the transesterification reaction 4000 times slower than heterogeneous base catalyst [14]. Therefore, heterogeneous base catalyst finds its best application in biodiesel production via transesterification [15]. So, present study has employed the heterogeneous basic catalysis in transesterification. Alkaline earth metals based catalysts are observed to be excellent heterogeneous basic catalysts in transesterification reaction for biodiesel production [16]. Among alkaline earth metals, the catalytic activity of elements in group (II) follows an ascending order with MgO < CaO < SrO ≤ BaO but lixiviation of BaO makes its application quite limited [17,18]. Hence strontium finds its place at apex in the series of active elements due to less relative loss from catalyst matrix [18,19]. Moreover strontium incorporates high charge density which ultimately provides the more number of basic sites for catalysis. Hence, it pacifies the generation of acyl acceptor by O–H bond cleavage in methanol which further forms fatty acid methyl ester (FAME). Many researchers demonstrated strontium oxide as a potential catalyst for various purposes [20,21]. Sr-Mg mixed metal oxides were successfully developed for methanolysis of palm oil [20]. The surface area and porosity of the Sr-Mg oxides were improved in comparison to the unsupported SrO. Strontium zirconate was synthesized by the citrate route in acidic medium and was evaluated as a potential heterogeneous catalyst for biodiesel production [22]. Chen et al. (2012) reported modified strontium with silica which resulted in refined olive derived biodiesel with 95% FAME in 10 min. Strontium and nickel oxides were exploited as heterogeneous catalyst synthesized by co-precipitation method and calcined at 1100 °C for 3 h [23]. The highest FAME conversion of 97% was achieved by using 2% of metal loading and oil/alcohol molar ratio of 1:9 at 65 °C in 5 h. Nevertheless, bare strontium based catalyst have been reported to undergo leaching to an extent during catalytic reaction. This phenomenon can be avoided by doping of active metal with some stable entities which can also synergies the transesterification reaction [23,24]. Here, titania can be introduced in crystal lattice in strontium based catalyst in order to stabilize the active site for sustainable catalysis. Hence in this work, a mixed metal oxide of Sr and Ti has been applied as solid base catalyst. Here, strontium acts as active element whereas titania is in synergistic role. Recently, titanium based materials have been applauded as dopant or support to active site in heterogeneous catalysis owing to their high surface area and chemical stability in mesoporous structure [25,26]. Furthermore, $TiO_2$ itself has gained the great attention as efficient metal oxide catalyst due to its strong metal support interaction, stability, and amphoteric chemical nature.

In present study, the mixed metal oxide of Sr and Ti ($SrTiO_3$) was prepared by sol–gel polymer precursor method [27] and its catalytic activity was evaluated in transesterification reaction for biodiesel production. The prepared catalyst underwent for several structural characterizations and got confirmed to inculcate the perovskite structure i.e. $SrTiO_3$. Perovskites are a family of mixed metal oxides which acquire the structural formula of $ABO_3$, where smaller transition metal ion resides on the B site, a centre of an octahedral geometry with O anions at corners, and bigger metal positions itself at A-site having 12-fold coordination with O anions [28]. Owing to the flexible electronic structure, perovskite catalyst exhibits manifold physical and chemical properties i.e. ferroelectricity, colossal magnetoresistance ion conductivity, anion-intercalation pseudocapacitors and oxygen ion diffusion [28,29]. This flexibility in electronic and crystal structure of perovskites makes them highly active, chemically versatile, selective, and stable catalysts. Recently, perovskites have gained tremendous application in reduction of fossil fuel emissions, decomposition of obnoxious materials, production of sustainable fuels and solid oxide fuel cells (SOFCs) [28]. In fact mixed metal oxide of strontium and titanium has been explored as catalyst for various applications in previous reports [30–32].

Apart from the catalyst, selection of feedstock for transesterification is the most critical task as fatty acid triglyceride from feedstock is converted into fatty acid methyl ester [2]. The feedstock should be widely available to be cost-effective as a large share of the biodiesel production cost comes from the feedstock value. In current study, mahua oil, a second generation non edible feedstock was consumed for biodiesel production. Recently, mahua oil has got greater importance due its abundance in nature and phenomenal growth. This plant is basically native to Indian sub-continental region. Its potential availability is estimated to 4,000,000 tons/year. Exclusively, mahua oil is extracted from its seed kernel containing 50–55% oil [33]. After processing the feedstock and synthesis of catalyst, they were fed up for transesterification reaction. Afterwards optimization of reaction influencing parameters such as catalyst dose, methanol to oil molar ratio, reaction temperature, reaction time were carried out to obtain the highest possible FAME conversion. All the valuable process parameters were taken into account and optimized through OVAT (One variable at a time) as well as RSM (response surface methodology) using Box Behnkehn Design (BBD). OVAT is simplest optimization technique which considers the variation of one factor at a time while keeping others constant in a reaction affected by multiple factors [14]. OVAT predicts about the linear effect of one variable on reaction while RSM seeks the possible interaction between variables affecting the reaction [34]. Next, a possible comparison of results from both the optimization technique was concluded in subsequent section. Ultimately, the compatibility of produced biodiesel with existing CI engine was ensured after evaluation of its fuel properties.

## 2. Materials and methods

### 2.1. Chemicals

Mahua oil was procured from market of the rural area nearby town. Strontium nitrate and titania were purchased from Alpha Aesar, U.K.; Acetone, bromothymol blue, benzoic acid, calcium chloride, calcium sulfate, cresol red, methyl red, neutral red, nile blue, sulphuric acid, phenolphthalein, sodium sulfate, and trapeolin were procured from Merck Ltd, Mumbai, India; citric acid, ethylene glycol, ethanol, and methanol were bought from SD FCL, Mumbai, India; potassium hydroxide and deuterated chloroform was acquired from SRL Pvt. Ltd. India.

### 2.2. Design of experiments

The optimization procedure was executed through OVAT and BBD, the statistical experimental design of RSM. OVAT allows the variation of one variable keeping others constant whereas BBD in RSM involves a simultaneous variation of process parameters. Statistically, RSM explores the possible correlation between considerable process parameters and process response [34]. In current work, BBD in RSM study was selected as an optimization design for biodiesel production through transesterification. Four independent process variables considered in RSM were catalyst dose ($X_1$), methanol to oil molar ratio ($X_2$), reaction temperature ($X_3$), and reaction time ($X_4$) at three steps (-1, 0, +1) enlisted in Table S1 (See supplementary). Here, a set of 27 experiments were conducted at process conditions generated by BBD using MINITAB 16 in Table S4 (See supplementary). The correlation between coded and uncoded process parameters was formulated in Eq. (1) [35].

$$\text{coded value} = \frac{\chi_i - \chi_n}{\Delta\chi} \quad (1)$$

where $X_i$ denotes the uncoded value of $i^{th}$ factor, $X_n$ presents the midway value of step, and $\Delta X$ is the interval. A second order polynomial relation between response and process variables is established as follows [36].

$$Y = \beta_0 + \sum_{i}^{4} \beta_i X_i + \sum_{i}^{4} \beta_{ii} X_i^2 + \sum \sum_{i<j=1}^{4} \beta_{ij} X_i X_j + \epsilon_r \quad (2)$$

where Y depicts the resultant response, i and j are the number of predicted process parameters.$\beta_0$, $\beta_i$, $\beta_{ii}$and $\beta_{ij}$ are the regression coefficient for intercept, linear, quadratic and interaction effect predicted by the method of least squares of individual variable [35,36], $\epsilon_r$ is the error involved in BBD prediction whereas $X_i$ and $X_j$ are the independent process variables. Analysis of variance regarding process variables was figured out on the basis of their linear, square and interactive effect on FAME conversion. The significant impact of process variables on the response was assessed by p and F values derived from ANOVA at a significant level of 0.05.

### 2.3. Catalyst preparation

The catalyst was prepared using sol–gel polymer precursor method [37–39]. Titanium oxide was taken as a titanium source while strontium was extracted from its nitrate precursor. The stipulated amount of metal precursors (2.1594 g of strontium nitrate and 0.8030 g of titania) was taken into the desired stoichiometric ratio (Sr/Ti of 1:1). Titania powder was thoroughly ultra-sonicated for 0.5 h which resulted in its uniform distribution throughout the reaction mixture. The polymer precursor of strontium was prepared by mixing above mentioned aqueous solution of alkaline earth metal precursor and equimolar amount of anhydrous citric acid with respect to metal precursors i.e. 3.84 g. Next equimolar amount of ethylene glycol to metal precursors was added to just above mentioned solution to facile the polymerization reaction via extensive intermetallic networking. Afterwards, this aqueous solution was gradually poured into the ultra-sonicated aqueous suspension of titania with continuous agitation of 500 rpm for 2 h at 80 °C. Onward, the entire reaction mixture having pH of 3.63 (acidic medium) was allowed to stand for a period of 4 h with continuous stirring at 90 °C resulting in formation of gel. Then dried material was fired at 350 °C. Finally, the resultant grey powder was thermally treated at 880 °C for 8 h to acquire the stable perovskite phase with no impurity.

### 2.4. Structure characterization and analytical methods

Thermal analysis of catalyst was carried out on SII 6300 EXSTAR with the heating rate of 10 °C/min starting from ambient temperature to 1000 °C. The phase identification and structural elucidation of prepared catalyst was made possible by X-Ray Diffraction observed on Rigaku XRD 600 Japan with Cu $K_\alpha$ radiation ($\lambda$ = 0.154 nm) over the 2θ range of 15°-90°. The elemental composition and the oxidation state of the Sr-Ti-O elements were ascertained by XPS employing PHI 5000 Versa Probe II, FEI, Inc model. The surface morphology along with elemental analysis of the prepared catalyst was conducted using Nova Nano SEM 450 Field Emission Scanning Electron Microscope (FESEM) combined with Energy Dispersive X-Ray Spectroscopy (EDS) unit. Transmission Electron Microscopy (TEM) image of $SrTiO_3$ particles was observed using a Tecnai G2 20 TWIN high-resolution transmission electron microscope inbuilt with selected area electron diffraction (SAED) unit at accelerating voltage of 200 kV. Fourier Transform Infra Red (FTIR) spectra of the catalyst samples were collected from Varian 3100 FTIR spectrometer in the range of 400–4000 $cm^{-1}$ using spectral-grade KBr pellets. Brunauer-Emmett-Teller (BET) surface area and Barret-Joyner-Halenda (BJH) pore size distribution were assessed by Micromeritics, ASAP 2020, USA. The basic sites residing on the surface of catalyst were quantified by Hammett indicator method [4,14]. Several indicators were employed for basicity check with $pK_{BH}^{+}$ in 6.51–11.84 (bromothymol blue, methyl red, neutral red, nile blue, phenolphthalein, and trapeolin). The produced biodiesel was analyzed by $^1$H NMR spectroscopy and ATR-FTIR spectroscopy. FAME in biodiesel was quantified from $^1$H NMR spectroscopy [4]. $^1$H NMR and $^{13}$C

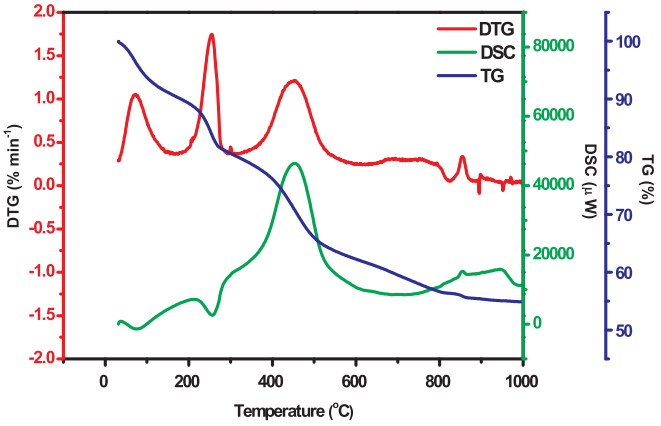


**Fig. 1.** TGA –DTA of crude catalyst.

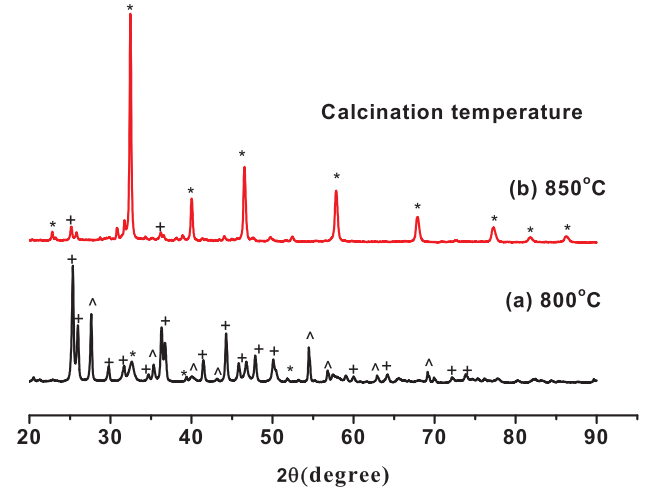


**Fig. 2.** XRD diffractogram of prepared catalyst at calcined 800 °C and 850 °C.

NMR spectra had been recorded on JEOL AL 300 instrument using TMS as an internal standard and deuterated chloroform as a solvent at the scan rate of 32. The ATR-FTIR spectrum of biodiesel was fetched on Alpha Bruker Eco-ATR mounted with ZnSe ATR crystal in the range of 500–4000 $cm^{-1}$ with 24 scans at a resolution of 2 $cm^{-1}$.

### 2.5. Batch experiments

The moisture content and suspended entities were removed from crude mahua oil. The free fatty acid (FFA) content was calculated in term of mg KOH/g using Eq. (3).

$$\text{Acid Value} = V_{KOH} * 56.1 * C_{KOH}/m_{sample} \quad (3)$$

Here $V_{KOH}$ and $C_{KOH}$ depict the volume and concentration of KOH in aqueous solution, respectively; $m_{sample}$ denotes the weight of mahua oil used.

The FFA value of 13.4 mg KOH/g was greater than 4 mg KOH/g limit suggested by ASTM [2,4,14]. Hence, a chemical pretreatment called esterification was executed to lessen FFA below the maximum limit. The suitable conditions optimized for acidic pretreatment by sulfuric acid were obtained as follows: catalyst dose; 1.5 wt%, methanol to oil molar ratio; 1:10, reaction temperature; 60 °C, reaction time; 90 min, and agitation speed; 600 rpm. The acidic esterification significantly lowered FFA value to 0.49 mg KOH/g. The FFA conversion was turn out to be 96% using Eq. (4).

$$\text{FFA Conversion}(\%) = (AV_1 - AV_2)/AV_1 * 100 \quad (4)$$

where $AV_1$ shows the acid value of feedstock (in mg KOH/g) and $AV_2$

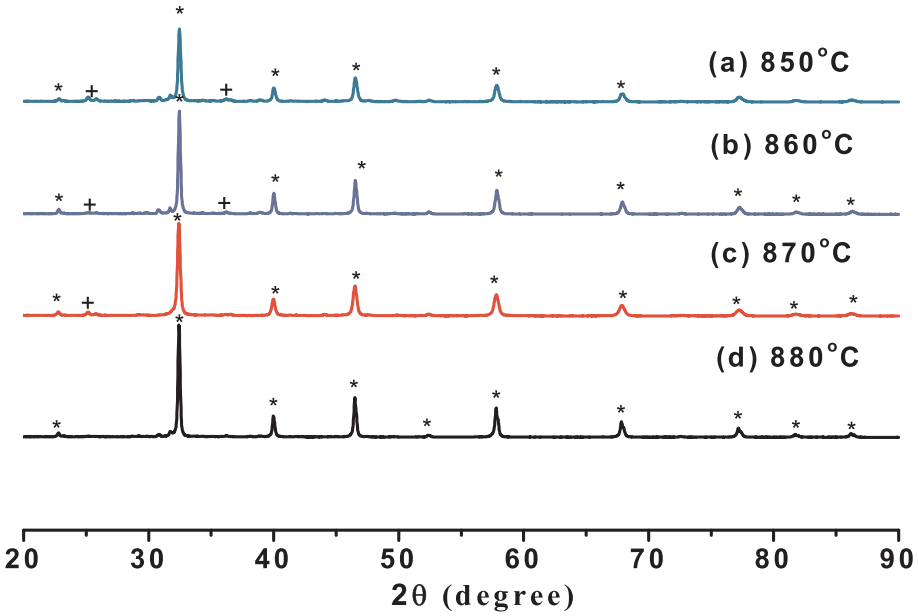


**Fig. 3.** XRD diffractogram of prepared catalyst calcined at 850 °C, 860 °C, 870 °C, 880 °C.

manifests the acid value of esterified feedstock (in mg KOH/g). Thereafter, esterified feedstock was fed for transesterification. The batch experiments of transesterification reaction were performed in three neck round bottom flask fitted with mechanical stirrer submerged in a temperature controlled water bath under reflux condition. The catalyst was uniformly dispersed in methanol with constant stirring at 60 °C for 0.5 h. Later, feedstock was added to it and the entire reaction system underwent for transesterification. Once, reaction got completed, biodiesel layer was separated from side products and catalyst. The catalyst was restored by multiple washing with n-hexane, methanol and ethanol to remove the organic residues and adsorbates away respectively. Additionally, chemisorbed clings were ejected out through thermal treatment at 600 °C for 2 h. Next, the regenerated catalyst underwent for transesterification reaction multiple times to explore to its reusability. The synthesized FAME was collected and further processed to remove the traces of methanol and moisture. The methyl ester conversion has been evaluated using Eq. (5) [14].

$$\text{FAME conversion}(\%) = (2\,A_{ME}/3A_{\alpha-CH2}) * 100 \quad (5)$$

where, $A_{ME}$ and $A_{\alpha\text{-}CH2}$ symbolize the integrated peak area of protons corresponding to methyl ester and methylene respectively. Moreover, optimization process was also executed out using methanol to oil molar ratio (3:1 to 1:23) and 0.3–2.3 wt% of the catalyst at reaction temperature (35-85 °C) for (20–180 min) reaction time with (500–800 rpm) agitation speed. The batch experiments for optimization of catalyst dose, methanol to oil molar ratio, reaction temperature, reaction time, and agitation speed were conducted using OVAT. These experiments rejected agitation speed as an effective process variable and thus, the effect of agitation speed was not considered in RSM experiments. Later, results obtained from both the optimization technique were compared accordingly. Additionally, experiments related to kinetics and thermodynamics were also carried out to describe the nature of mechanism followed in transesterification.

### 2.6. Kinetics and thermodynamic investigation of transesterification

The suitable kinetic model for methanolysis was developed by employing the best reaction conditions for higher ester transformation in biodiesel production. The reaction kinetics for heterogeneous catalysis could not be comprehended so well as in case of homogeneous catalysis. As heterogeneous methanolysis occurs in various physicochemical steps and in triphasic system comprising a solid catalyst and two immiscible liquid phases. But efforts were made to avoid the intra-particle and mass transfer resistance by providing nano-catalyst and ideal stirring conditions to reaction system. Considering the chemical process, rate limiting step, the pseudo-first-order kinetic model was prominently reported in literature for biodiesel production in methanolysis [4]. Ideally, transesterification process consumes 1 mol of and 3 mol of methanol and results 3 mol FAME and 1 mol of glycerol, side product [14]. Accounting transesterification, a tetra-molecular elementary reaction, the rate law can be expressed as follows.

$$r = -\frac{d[TG]}{dt} = k'[TG][M]^3 \quad (6)$$

where k', [TG], and [M] designate the rate constant, triglyceride concentration and methanol concentration, respectively. According to rate law expression in Eq. (6), methanolysis was observed to follow the fourth order rate law. But the reversible nature of transesterification reaction compelled the usage of excess methanol to drive the reaction in the forward direction. The addition of excess methanol avoided the chances of reverse reaction. Since change in concentration of methanol was supposed to be constant throughout the process, this limited the reaction mechanism to follow the pseudo-first-order kinetics [14]. Finally, the reaction rate only depended on triglyceride concentration. Thus pseudo-first-order rate law expression could be formulated as Eq. (7) [40,41].

$$r = -\frac{d[TG]}{dt} = k[TG] \quad (7)$$

Now k exhibits revised rate constant

$$k = k'[M]^3 \quad (8)$$

After integrating Eq. (7)

$$\ln[TG_0] - \ln[TG] = kt \quad (9)$$

Applying mass balance for methyl ester conversion

$$M_E = 1 - \frac{[TG]}{[TG_o]} \quad (10)$$

Here, $M_E$ depicts methyl ester conversion

$$[TG] = [TG_0](1 - M_E) \quad (11)$$

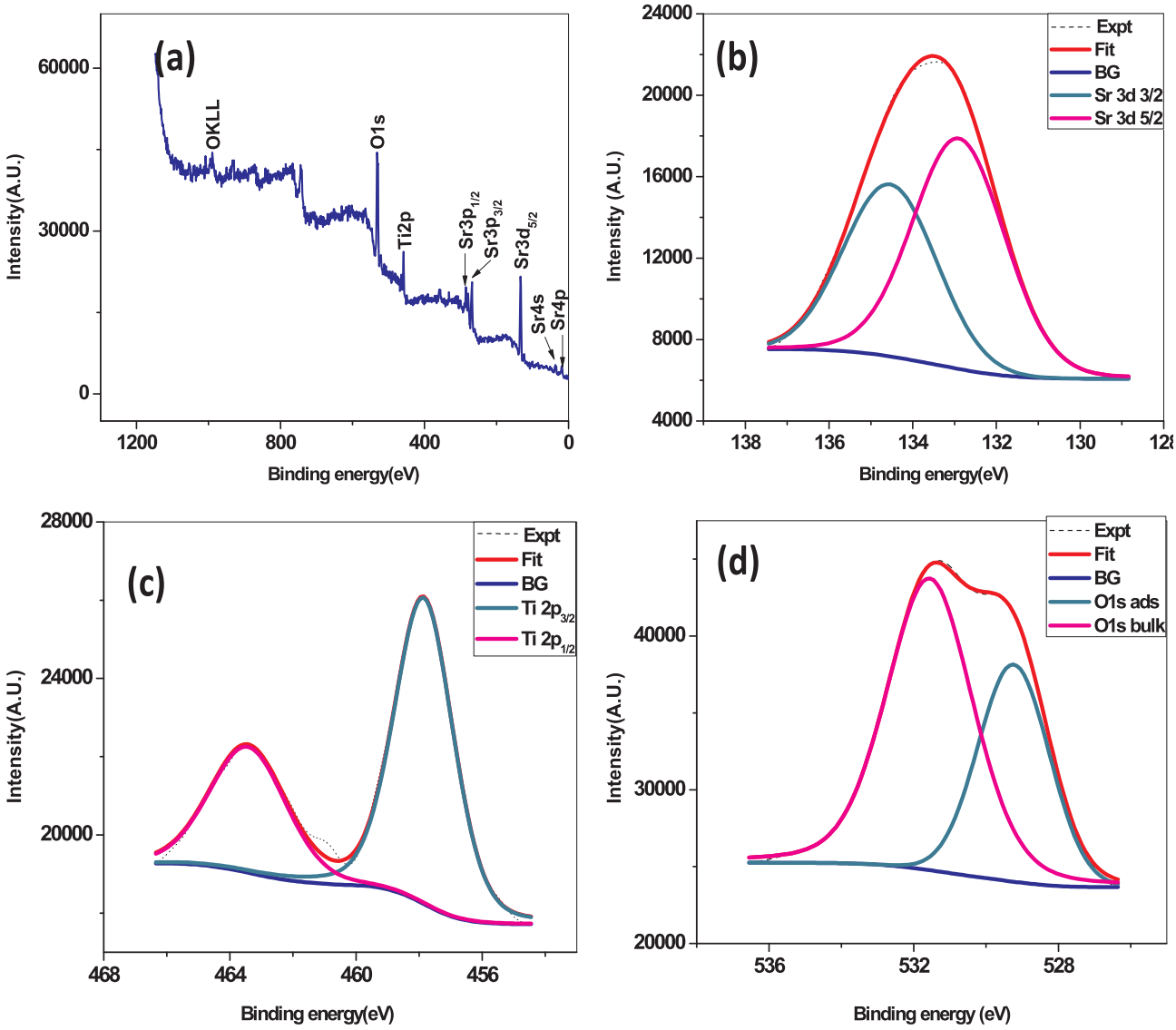


**Fig. 4.** XPS analysis of strontium titanate (a) wide scan full spectrum of $SrTiO_3$, (b) Sr XPS 3d spectra, (c) Ti XPS 2p spectra, (d) O XPS 1 s spectra.

$$\frac{d[M_E]}{dt} = k(1 - M_E) \tag{12}$$

$$-\ln(1 - M_E) = kt \tag{13}$$

Eq. (13) represents the first order kinetic expression of -ln(1-$M_E$) versus t for the evaluation of rate constant at different reaction temperatures. The activation energy ($E_a$) and frequency factor (A) for methanolysis of mahua oil were determined from Arrhenius equation [42].

$$k = A\exp(-E_a/RT) \tag{14}$$

The logarithmic form of Eq. (14) can be written as follows.

$$\ln\ k = \ln\ A - E_a/RT \tag{15}$$

where k displays rate constant resulted from Eq. (13) using pseudo-first-order kinetic model. A, R, T, and $E_a$ show the frequency factor, the universal gas constant (8.314 J/mol/K), the absolute temperature (K) and the activation energy of transesterification, respectively. Thermodynamic parameters including enthalpy change ($\Delta H^\circ$), entropy change ($\Delta S^\circ$) and Gibb's free energy change ($\Delta G^\circ$) could be calculated using Eyring-Polanyi expression given as follows [43].

$$k = \frac{k_b T}{h}\exp\left(-\frac{\Delta G^\circ}{RT}\right) \tag{16}$$

Taking log of Eq. (16) and substituting $\Delta G^o$ into fundamental thermodynamic equation provided as below:

$$\Delta G^\circ = \Delta H^\circ - T\Delta S^\circ \tag{17}$$

Eq. (16) could be rearranged into the following expression.

$$\ln\left(\frac{k}{T}\right) = -\left(\frac{\Delta H^\circ}{RT}\right) + \left[\ln\left(\frac{k_b}{h}\right) + \frac{\Delta S^\circ}{R}\right] \tag{18}$$

where k is the rate constant ($min^{-1}$); T is the absolute temperature (K); R is the universal gas constant; h and $k_b$ represent as Planck's constant ($6.626 \times 10^{-34}$ J/s) and Boltzmann's constant ($1.38 \times 10^{-23}$ J/K), respectively.

## 3. Results and discussion

### 3.1. Feedstock

The fatty acid component profile was already examined through GC–MS in our previous work [14]. However, the prominent fatty acids found are enlisted in Table S2 (See supplementary). GC–MS analysis of mahua oil has shown following fatty acid distribution: hexadecanoic acid; 9,12-octadecadienoic acid; 9-octadecenoic acid; 9-hexadecenoic

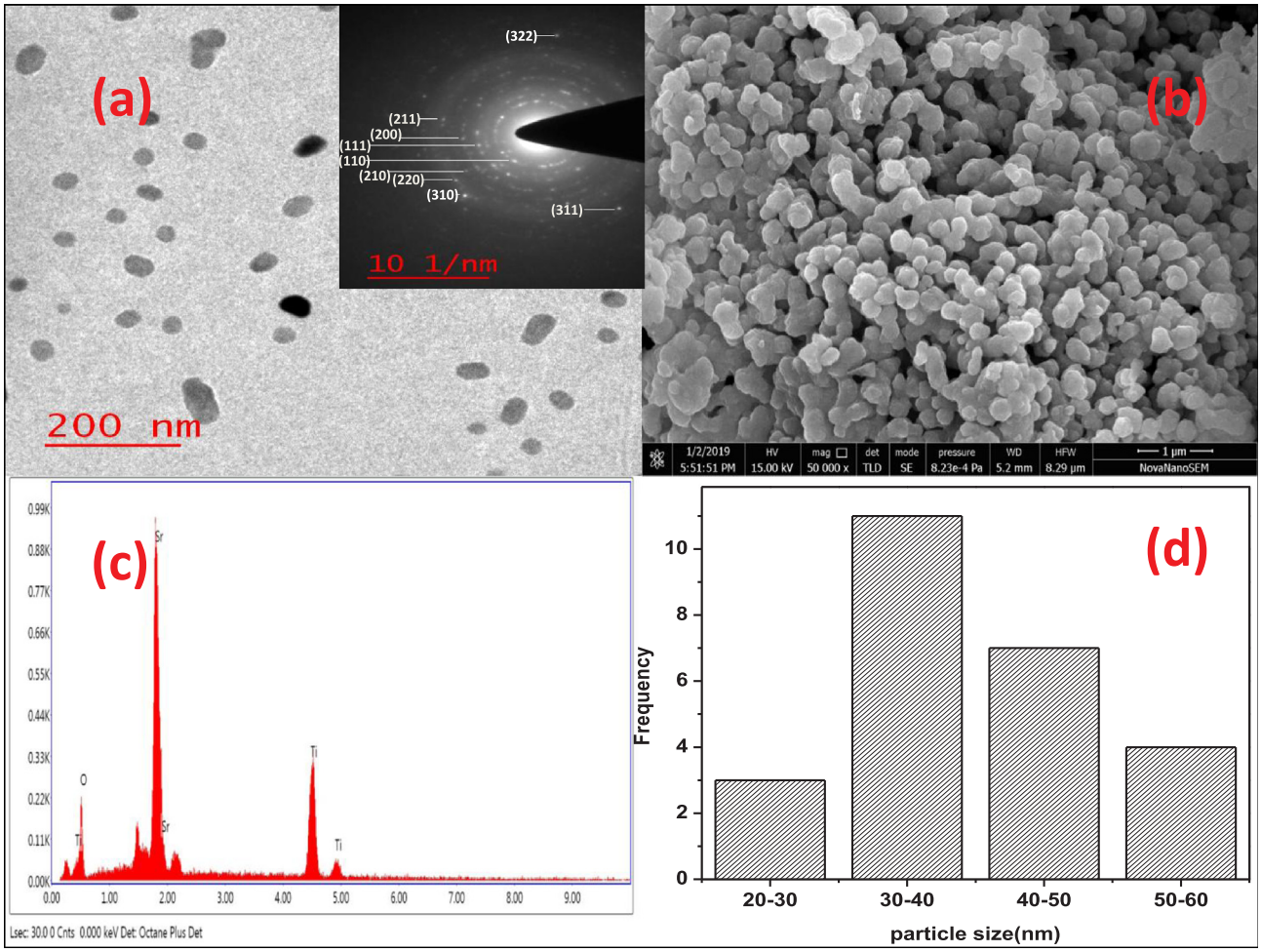


**Fig. 5.** (a) TEM image of $SrTiO_3$ (b) FESEM image, (c) EDAX histogram of $SrTiO_3$, (d) particle size analysis of $SrTiO_3$ inferred from TEM image, (e) SAED pattern of $SrTiO_3$.

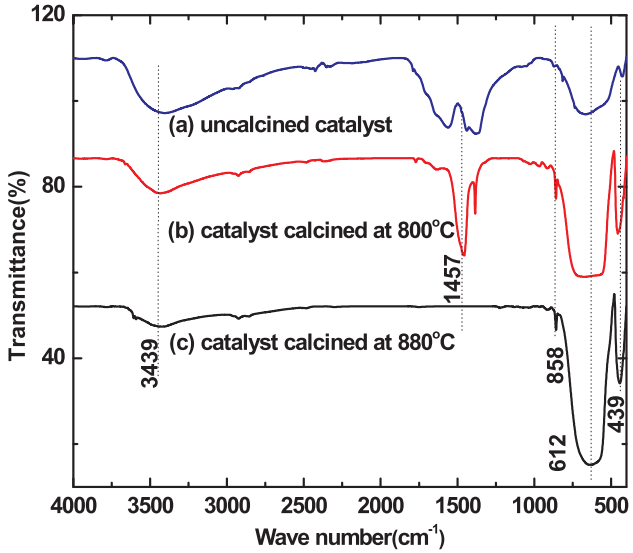


**Fig. 6.** FTIR spectra of prepared catalyst calcined at different temperature.

acid; Icosanoic acid. 9,12-octadecadienoic acid was found to be the prominent component of triglyceride content. Similar composition was also observed in previous studies [44,45].

### 3.2. Catalyst

The physicochemical characteristics of catalyst were deciphered by several characterizations discussed in following subsections.

#### 3.2.1. tGA/DSC/DTG

The crude catalyst was examined for its thermal response over a wide temperature range. DTG curve showed four consecutive mass losses at 74 °C, 255 °C, 451 °C and 815 °C occurring with degradation rate of 1.052%/min, 1.745%/min, 1.209%/min and 0.235%/min respectively. The TGA-DSC-DTG plots in Fig. 1 also present four consecutive mass loss events. The first weight loss was about 11.4% in the range from room temperature to 189 °C which is characterized by an endothermic phenomenon. It is attributed to the dehydration of adsorbed water from adsorbent surface [41] since catalyst is found to be hygroscopic. The second weight loss about 11.1% occurred in the range of 200–350 °C manifested by an endothermic peak in DSC owing to degradation of nitrates and organic volatiles from crude catalyst [4,14]. The next mass loss is attributed to an exothermic event owing to the evolution of CO and $CO_2$ as a result of combustion organic matters which happened in the temperature range of 450-698 °C with 17% mass loss. Afterward, the last fourth one found to be an exothermic step rendered from ~700 °C to 845 °C involving 5.5% mass loss regarding combustion of the residual carbon, degradation of metal carbonate and crystallization [46] of the catalyst with perovskite structure formation.

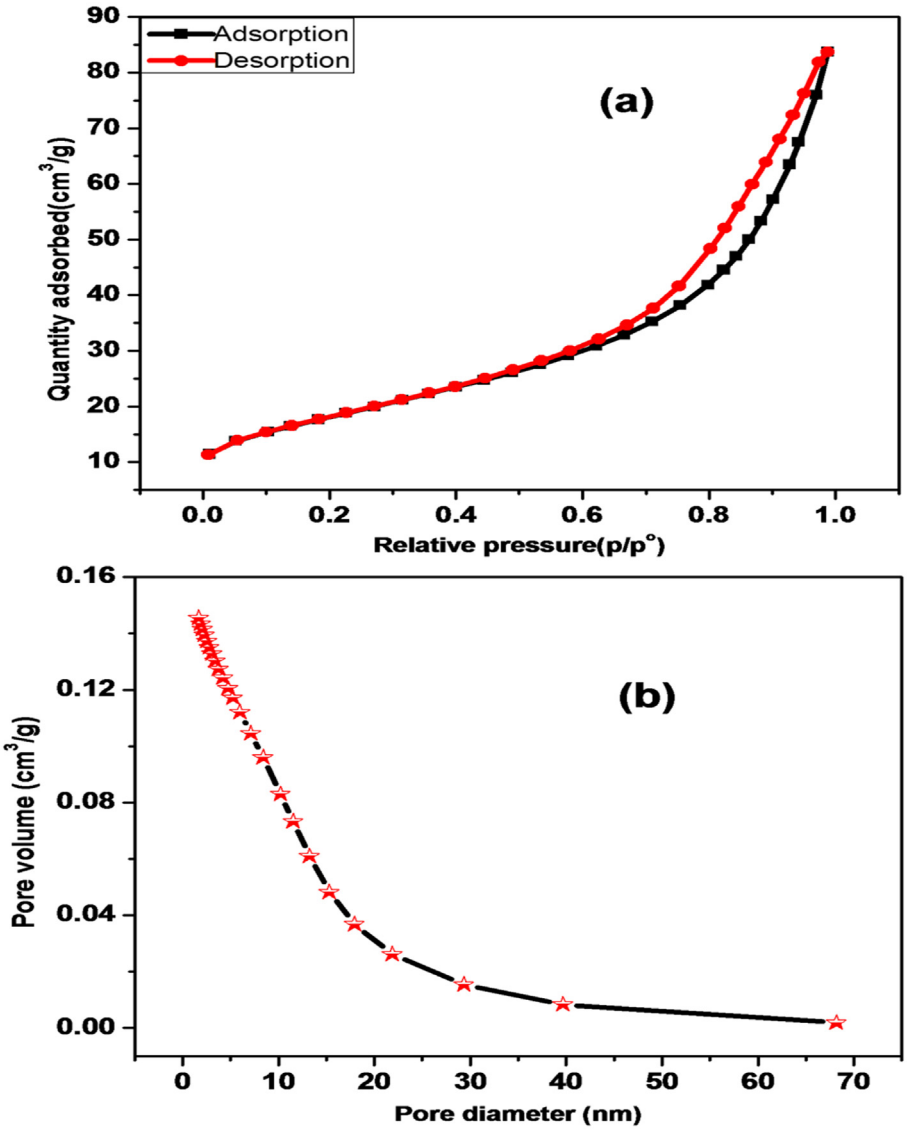


**Fig. 7.** (a) $N_2$ adsorption–desorption profile of the catalyst; (b) BJH adsorption pore size distribution of the catalyst.

*3.2.2. xRD*

The crystallinity and phase purity of the prepared perovskite were examined using X-ray diffraction. Since thermal degradation pattern could not clearly infer the calcination temperature, this ambiguity was resolved after thermal treatment at different temperatures (800 °C, 850 °C, 860 °C, 870 °C, 880 °C) to obtain the desired perovskite structure. Fig. 2 & Fig. 3 illustrate the X-Ray diffractogram of catalyst calcined at different temperatures. The calcination at 800 °C did produce the catalyst with two major metallic phases $SrCO_3$ (prominent peaks positioned at 25.19°(1 1 1), 25.83°(0 2 1), 29.65°(0 0 2), 31.54°(0 1 2),35.137°(2 0 0), 36.56°(1 3 0), 41.31°(2 2 0), 44.12°(1 3 2), 49.51°(1 4 1), 50.19°(1 1 3), 57.31°(3 1 1), and 59.93°(1 5 1) also existing in JCPDS file #712393) and $TiO_2$ (prominent peaks positioned at 27.31°(1 1 0), 35.86°(1 1 0), 39.1°(2 0 0), 40.98°(1 1 1), 54.02°(2 1 1), 56.37°(2 2 0), and 63.71°(3 1 0) detailed in JCPDS file#896975) with some traces of $SrTiO_3$ observed peaks at 32.4°(1 1 0) and 46.5°(2 0 0). But, further increase by 50 °C in temperature raised the peak intensity of the perovskite phase with intensity deterioration in others phase shown in Fig. 2. This XRD pattern described that native metals oxides insertion into each other to form compact perovskite structure was started from 800 °C and completed at 850 °C but with a trace of residual strontium carbonate.

$SrCO_3$

→ SrO(carbonates degradation followed by native metal oxide insertion)

$SrO + TiO_2 \rightarrow SrTiO_3$(perovskite formation)

The complete formation perovskite phase with structural formula $SrTiO_3$ was observed at 880 °C in Fig. 3 showing the presence of high intensity peaks with 2θ values of 22.7°(1 0 0), 32.4°(1 1 0), 39.9°(1 1 1), 46.5°(2 0 0), 52.3°(2 1 0), 57.8°(2 1 1), 67.8°(2 2 0), 77.2°(3 1 0), 81.7°(3 1 1), and 86.2°(2 2 2) reported in JCPDS file# 894934. The samples calcined at some other temperature has incorporated some sort of impurities arrived in terms of residual peaks. The crystallite size was also calculated using following Debye Scherer formula [47].

$$d = \frac{K\lambda}{\beta\cos\theta} \tag{19}$$

where d represents the mean crystallite size of the catalyst which might be equal to all smaller than particle size. K is a unit less shape factor whose value is of about 0.9, but varies with crystallite actual shape; λ is the wavelength of X-ray (1.54 nm); β is the line broadening at FWHM (in radians); θ is the diffracting Bragg angle. The crystallite size calculated to be 30.78 nm. This specifies the catalyst as nano-catalyst. The smaller particle size offered higher surface area which was the ultimate

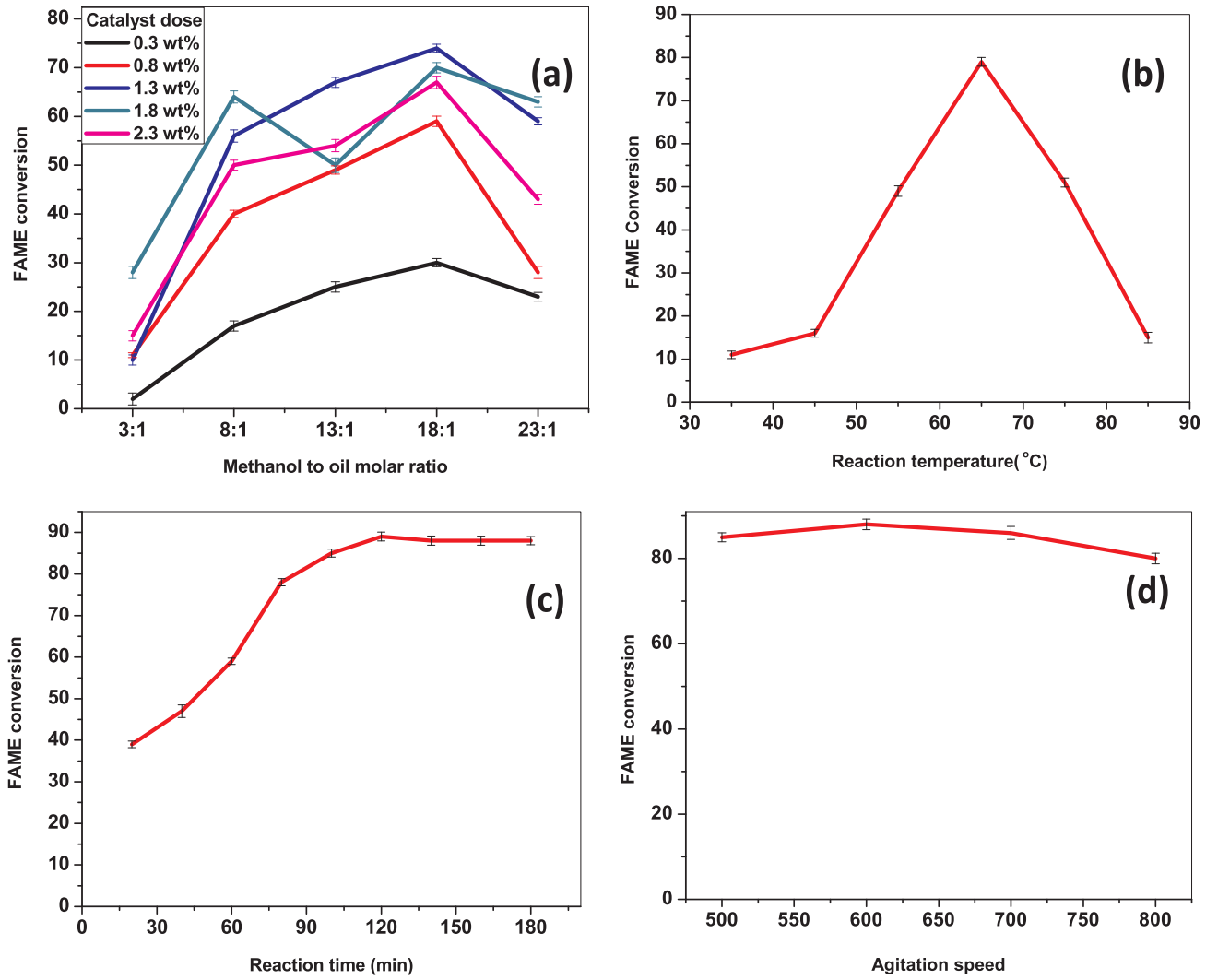


**Fig. 8.** Optimization plots manifesting (a) Effect of alcohol to oil molar ratio alongwith different catalyst dose on FAME conversion (reaction temperature: 60 °C; reaction time: 2.5 h; agitation speed: 500 rpm). (b) Effect of reaction temperature on MOME conversion (catalyst dose: 1.3 wt%; oil to alcohol molar ratio: 1:18; reaction time: 2.5 h; agitation speed: 500 rpm). (c) Effect of reaction time on MOME conversion (catalyst dose: 1.3 wt%; oil to alcohol molar ratio: 1:18; reaction temperature: 60 °C; agitation speed: 500 rpm). (d) Effect of agitation speed on MOME conversion (catalyst dose: 1.3 wt%; oil to alcohol molar ratio: 1:18; reaction temperature: 60 °C; reaction time: 2 h).

reason for the catalytic activity of prepared strontium titanate.

### 3.2.3. xPS

X-ray photoelectron spectroscopy analysis was carried out to extract the detailed information regarding elemental composition, chemical, electronic state, and the oxidation state of the Sr-Ti-O elements. A typical survey XPS spectrum of perovskite material was illustrated in Fig. 4a, in which characteristic peaks of Sr, Ti, and O elements were all present. Fig. 4b represents Sr 3d core level spectra of bulk $SrTiO_3$. Due to the Sr 3d spin orbit-splitting, the single experimental peak is fitted to two prominent peaks regarding to two characteristic peaks (Sr $3d_{3/2}$ and Sr $3d_{5/2}$) positioned at 134.6 eV and 132.9 eV respectively. The peaks position of Sr $3d_{5/2}$ substantiated the +2 bulk oxidation state of strontium in perovskite structure [48]. This binding energy information of Sr agrees well with Sr $3d_{3/2}$ and Sr $3d_{5/2}$ positions reported for bulk Sr 3d [48]. Fig. 4c shows the Ti 2p core level of $SrTiO_3$ excited by $AlK_\alpha$ radiation. Here again, the two peaks have been obtained because of spin–orbit splitting generating $2p_{3/2}$ and $2p_{1/2}$. The characteristic peak of Ti $2p_{3/2}$ peak occurs at 457.6 eV with FWHM 2.1 eV. The observed positions of Ti $2p_{3/2}$ and Ti $2p_{1/2}$ peaks are in the close agreement with the reported values of $Ti^{4+}$ [49]. The XPS spectrum of O 1 s core level of bulk $SrTiO_3$ excited by $AlK_\alpha$ radiation is depicted in Fig. 4d. The broad spectrum of O 1 s is fitted into two peaks one at 529.2 eV with FWHM of 2.6 eV and the other at 531.5 eV associated with FWHM of 3.1 eV. The former is attributed to adsorbed oxygen or hydroxyl species as $SrTiO_3$ is hygroscopic, it can absorb water from ambient and from hydroxyl species while the latter one corresponds to stoichiometric oxygen in the catalyst sample [49].

### 3.2.4. Morphological analysis

The structural characteristics and morphology of perovskite $SrTiO_3$ was examined by FESEM and TEM equipped with SAED. TEM micrograph of catalyst in Fig. 5a revealed the formation of spherical strontium titanate while SAED pattern (inset) was observed to further substantiate the finding from XRD analysis of catalyst by correlating the lattice parameters (*d* spacing) of the $SrTiO_3$ catalyst reported in Fig. 5e. A consecutive SAED pattern of circular diffused fringes with bright spots revealed $SrTiO_3$ as nanocrystalline catalyst. Additionally, the bright spots in the SAED pattern are attributed to the lattice plane indexed by (1 1 0), (1 1 1), (2 0 0), (2 1 0), (2 1 1), (2 2 0), (3 1 0), (3 1 1) and (3 2 2) also observed in X-Ray diffractogram (Fig. 3) with noticeable intensity. The particle size was calculated in Fig. 5d using Image-J

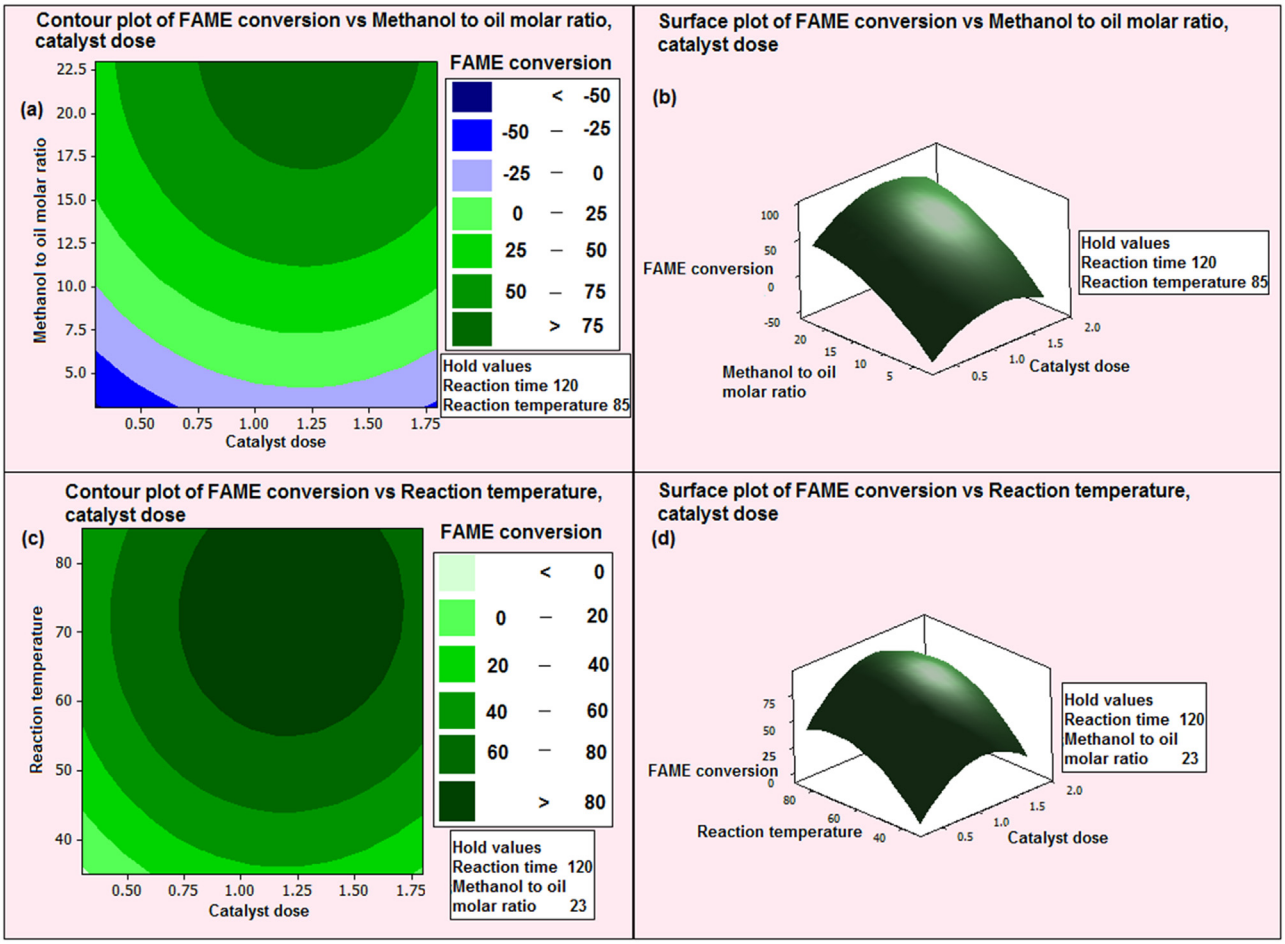


**Fig. 9.** (a) Contour plot of FAME conversion vs methanol to oil molar ratio, catalyst dose at hold values of reaction time (1 2 0) and reaction temperature (85 °C),(b) Surface plot of FAME conversion vs methanol to oil molar ratio, catalyst dose at hold values of reaction time and reaction temperature (85 °C), (c) Contour plot of FAME conversion vs reaction temperature, catalyst dose at hold values of reaction time and methanol to oil molar ratio (23), (d) Surface plot of FAME conversion vs reaction temperature, catalyst dose at hold values of reaction time and methanol to oil molar ratio (23).

and found to be in the nano-range confirming the formation of strontium titanate nanospheres [48,50]. Fig. 5b illustrates the surface morphology of $SrTiO_3$. Fig. 5b evinces the formation of strontium titanate nanospheres with approximately uniform particle size. EDS histogram in Fig. 5c informed the elemental composition of prepared catalyst. It validated the structural formula of $SrTiO_3$ confirmed by XRD. The information regarding elemental profile of synthesized $SrTiO_3$ catalyst from EDS histogram is enlisted in Table S3 (See supplementary).

### 3.2.5. fTIR

Fig. 6 exhibits the FTIR spectra of uncalcined catalyst and calcined catalyst at 800 °C and at 880 °C for 8 h, respectively. The FTIR spectrum of $SrTiO_3$ was quite similar to that of $SrTiO_3$ reported previously [51]. The broad band at 3439 $cm^{-1}$ exhibits O–H stretching modes of chemisorbed water molecule by KBr pellets that were used for FT-IR spectroscopy [48]. The broad band at ~ 1457 $cm^{-1}$ in Fig. 6a and b can be interpreted as C = O vibration due to the extremely unavoidable presence of metal carbonate [14,48]. The intensity of this peak was assuaged with an increase in temperature due to the removal of metal carbonates as in Fig. 6c. Bands at 858 $cm^{-1}$ and 612 $cm^{-1}$ were due to octahedron $TiO_6$ stretching and bending vibration, respectively [48,50]. The characteristic high-intensity peak at 612 $cm^{-1}$ in Fig. 6c confirms the strontium titanate structure substantiating the XRD results [52]. Fig. 6c represents the IR spectrum of strontium titanate exhibiting only characteristic peaks of existing bond vibrations. This may be due to the purity, crystallinity and particle size of powder calcined at 880 °C.

### 3.2.6. BET surface area

Nitrogen adsorption and desorption measurements were performed to estimate BET surface area and BJH pore size distribution of the prepared catalyst. $S_{BET}$ surface area has been determined as 39.0 $m^2/g$. The pore diameter and the pore volume were calculated to be 7.638 nm and 0.144 $cm^3/g$ respectively. The pore size distribution of strontium titanate classified the catalyst as mesoporous material. The compatibility of the pore diameter (7.638 nm) and size of the triglyceride molecule (≈ 6 nm) eases the diffusion of triglyceride molecule onto the surface of catalyst [14,16]. The linear isotherm profile (IV type) of the strontium titanate (Fig. 7a) corroborates the results from the pore size distribution with hysteresis (type III) (Fig. 7b), a characteristic feature of mesoporous materials [53]. Finally, surface area characterization of the catalyst ensures the catalyst have got sufficient active sites to catalyze the transesterification.

### 3.2.7. Basicity

Heterogeneous basic catalysts comprise Bronsted and Lewis basic sites existing on their surface which are responsible for their basic strength [12]. Hammett indicator- benzene carboxylic acid titration method was employed for basicity measurement of prepared solid catalyst. The benzene solution of catalyst sample was titrated against benzoic acid using several indicators having $pK_{BH+}$ in between 6.51 and 11.84 (bromothymol blue, methyl red, nile blue, neutral red,

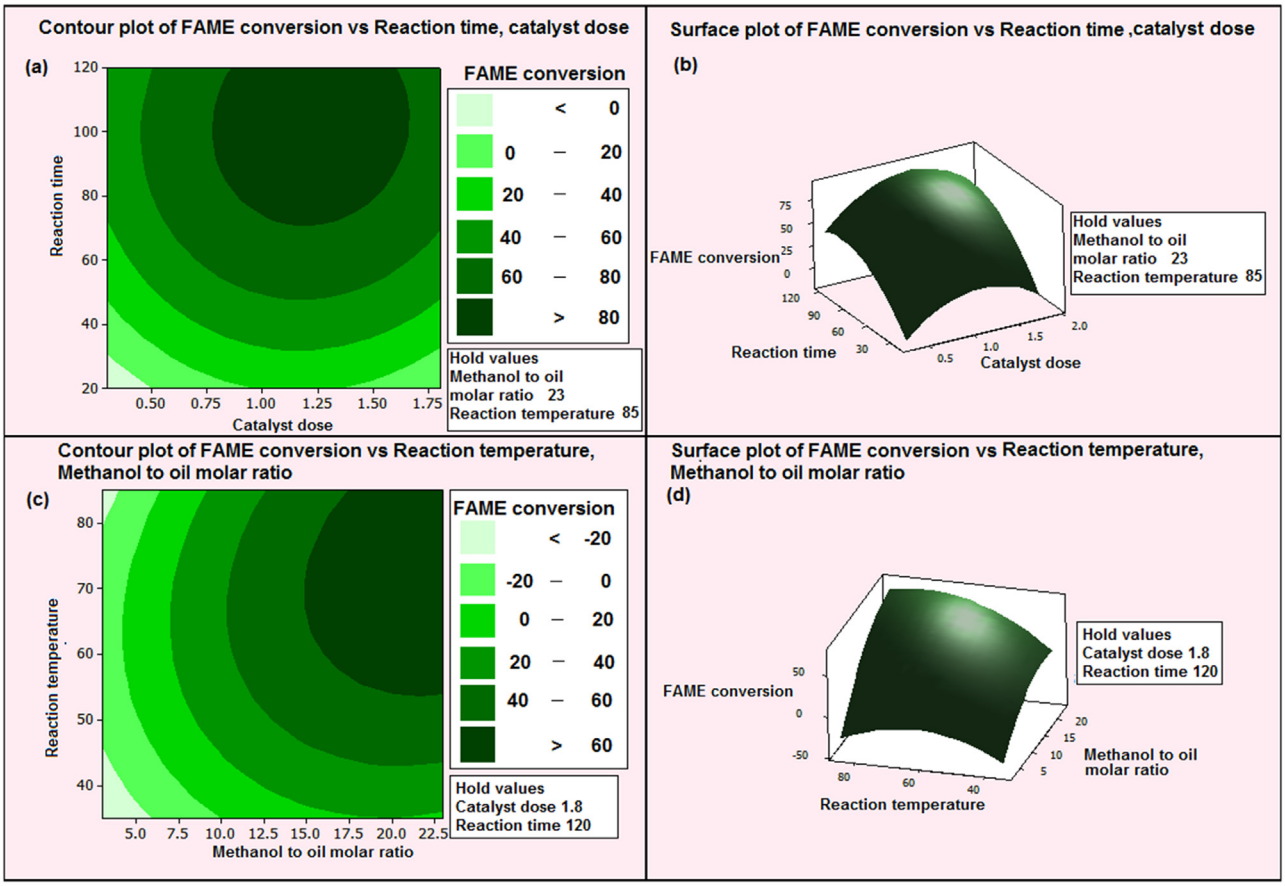


**Fig. 10.** (a) Contour plot of FAME conversion vs reaction time, catalyst dose at hold values of methanol to oil molar ratio (23) and reaction temperature (85 °C),(b) Surface plot of FAME conversion vs reaction time, catalyst dose at hold values of methanol to oil molar ratio (23) and reaction temperature (85 °C) (c) Contour plot of FAME conversion vs reaction temperature, methanol to oil molar ratio at hold values of catalyst dose (1.8%) and reaction time, (d) Surface plot of FAME conversion vs reaction reaction temperature, methanol to oil molar ratio at hold values of catalyst dose (1.8%) and reaction time .

phenolphthalein and trapeolin). The total basicity of strontium titanate was found to be 1.89 mmol/g.

### 3.3. Optimization of process parameters

The major factors including catalyst dose, methanol to oil molar ratio, reaction temperature, reaction time and agitation speed, were considered for the optimization process in order to obtain the highest methyl ester conversion [54].

#### 3.3.1. oVAT

Initially, series wise experiments were performed to find out the extreme range of each process variable in the transesterification reaction. In OVAT, optimization was processed over the range of individual variable: 0.3–2.3 wt%; catalyst dose, 3:1–23:1; methanol to oil molar ratio, 35 °C – 85 °C; reaction temperature, 20–180 min; reaction time, 500–800 rpm; agitation speed. In the following figure, optimization of catalyst dose along with methanol to oil molar ration was performed. Though transesterification reaction stoichiometrically needs only 3:1 methanol to oil molar ratio but still exorbitant methanol must be supplied to push this reaction in the forward direction [55]. Besides, non-edible feedstock urges higher methanol to molar ratio to lessen the fluid viscosity [56]. Additionally, catalyst facilitates the reaction by adopting the new path of low activation energy by rendering the reaction site on its surface which facile the interactions between reacting molecules [57]. OVAT predicted the maximum methyl ester conversion of- 90% at optimum reaction conditions using 1.3 wt% catalyst dose with 18:1 methanol to oil molar ratio (Fig. 8a) at 60 °C for 2 h. Predominantly, excess catalyst increases fluid viscosity which terminates the molecular interaction necessary for FAME production [54]. The higher methanol to oil molar ratio dilutes the catalytic concentration at the same time and makes the biodiesel separation from glycerin more difficult [58,59]. The temperature always has a strong kinetic effect on the reaction mechanism. Fig. 8b illustrates that after boiling temperature of methanol methyl ester conversion starts depleting [59]. This regards to the evaporation of methanol from the reaction system which makes the contact between catalyst and methanol more difficult hence lowers the biodiesel production. The reaction time was optimized as in Fig. 8c by monitoring the reaction over the appreciable length of time. The reaction mixture was arrested at different time intervals and $^{1}$H NMR was recorded to monitor the FAME conversion. The optimized for present study was found to be 120 min. After that biodiesel production was almost constant. It has been seen that keeping reaction mixture under vigorous agitation for a longer period makes the biodiesel separation a bit difficult as the glycerol layer start dissolving in the glycerin phase [60]. The effect of stirring was also checked and its effect overseen (Fig. 8d) was noted inappreciable to any extent. So, OVAT suggested catalyst dose, methanol to oil molar ratio, reaction temperature, and reaction time as dominating process parameters. Therefore, only these factors have been taken into consideration in the RSM study.

#### 3.3.2. rSM

Regression model equation for response in methanolysis has been reckoned by assessing the following process variables namely catalyst dose, alcohol to oil molar ratio, reaction temperature and reaction time. All process variables coefficients were computed from the experimental

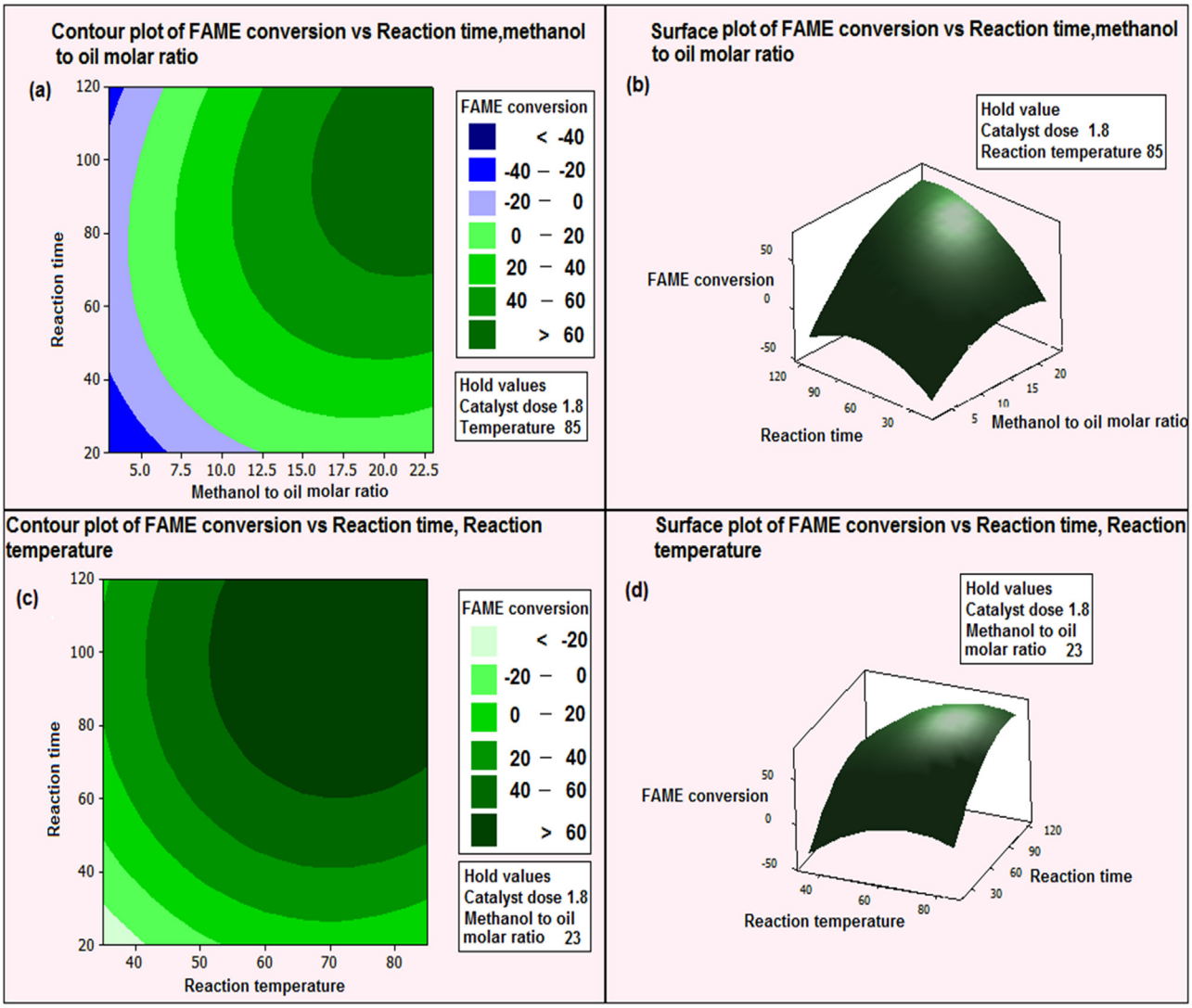


**Fig. 11.** (a) Contour plot of FAME conversion vs reaction time, methanol to oil molar ratio at hold values of catalyst dose (1.8%) and reaction temperature(85 °C),(b) Surface plot of FAME conversion vs reaction time, methanol to oil molar ratio at hold values of catalyst dose (1.8%) and reaction temperature (85 °C) (c) Contour plot of FAME conversion vs reaction time, reaction temperature at hold values of catalyst dose (1.8%) and methanol to oil molar ratio (23), (d) Surface plot of FAME conversion vs vs reaction time, reaction temperature at hold values of catalyst dose (1.8%) and methanol to oil molar ratio (23).

data elucidated in Table S4 (See supplementary) and Table S5 (See supplementary). BBD in this RSM study was applied to estimate the correlation between the process variables and the FAME conversion. The following regression equation was yielded after the regression analysis of selected coded terms in transesterification for FAME conversion.

$Y = -192.520 + 104.967$ (catalyst dose) + 2.917(methanol to oil molar ratio) + 4.085(reaction temperature) + 1.004(reaction time) − 51.704(catalyst dose × catalyst dose) −0.212(methanol to oil molar ratio × methanol to oil molar ratio) −0.039(reaction temperature × reaction temperature)-0.010(Reaction time × reaction time) + 0.167(catalyst dose × methanol to oil molar ratio) + 0.107(catalyst dose × reaction temperature) + 0.080(catalyst dose × reaction time) + 00.044(methanol to oil molar ratio × reaction temperature) + 0.030(methanol to oil molar ratio × reaction time)

The greater value of regression coefficient (greater than80%) denotes the good fit of the regression model [34]. In this study of BBD, the value of $R^2$ was found to be 95.52% with $R^2$ (adj) to be 90.29%. Aforementioned values of $R^2$ manifests that the quadratic model is valid to explain the factorial influence of process parameters in transesterification for biodiesel production. The individual terms having probability value more than 0.05 are considered to be non-significant. Therefore, catalyst dose, methanol to oil molar ratio, reaction temperature and reaction time were found to be the indispensable factors genuinely affecting the transesterification process. The square effects of each term were also quite significant. The behavior of an individual term is manifested by the positive or negative sign of its coefficient value. The catalyst dose, methanol to oil molar ratio, reaction temperature and reaction time had positive coefficients which meant that FAME conversion increased with these process variables. The above-mentioned trend is also substantiated by OVAT for inceptive values of process parameters before the saturation limit of FAME conversion. The impact of each process parameter is assessed by its coefficient magnitude. So, catalyst dose is assessed to be the strongest factor among all other existing parameters.

*3.3.2.1. Analysis of variance.* Analysis of variance (ANOVA) validates the approach of the quadratic model which has been utilized to establish the appropriate relationship among process variables. The extracted consequences from RSM were analyzed by ANOVA and Fisher's statistical test (F-test) suggested the quadratic model to be the best fit tabulated in Table S6 (See supplementary). The calculated

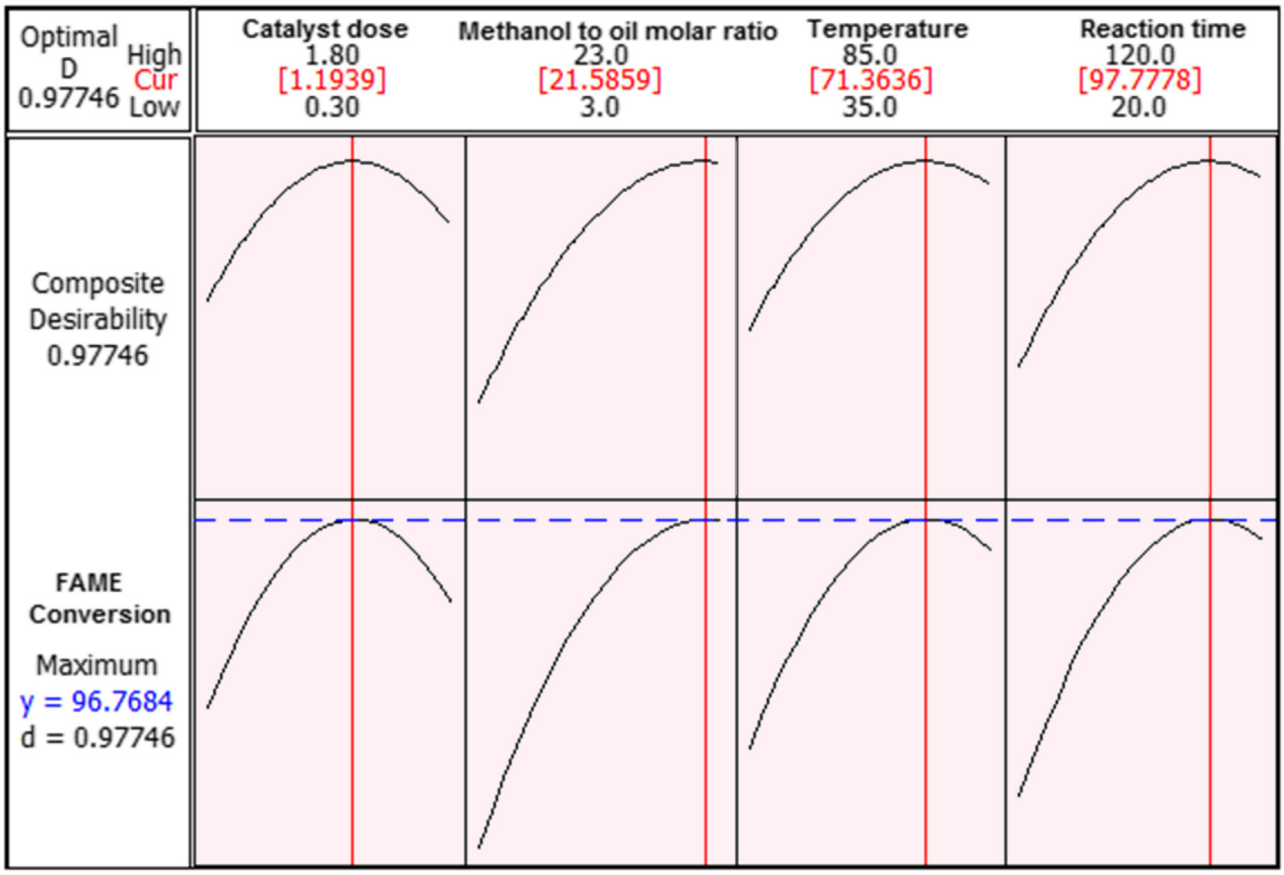


**Fig. 12.** Optimization plot of process variables in transesterification reaction for biodiesel production using strontium titanate.

probability of terms < 0.05 is considerable. Hence catalyst dose was obtained to be the most influencing parameter followed by reaction temperature, reaction time and methanol to oil molar ratio. Considering the square effects in Table S6 (See supplementary), the catalyst dose was again perceived as the most significant factor. Next, the reaction temperature was the next noteworthy factor after catalyst dose (on the basis of the sum of squares) followed by reaction time and methanol to oil molar ratio.

*3.3.2.2. Outcomes from RSM.* Graphical interpretation of the interaction of variables is executed by response plots i.e. contour plots and surface plots. 3D surface and contour plots give the idea about the interaction between independent variables alongwith response of the transesterification according to experimental design. The conversion is initially raised with catalyst dose as well as with methanol to oil molar ratio but after achieving certain limit; it started lowering down as exp. no. (1, 2, and 25) and (2, 3, and 26). This is also supported by OVAT. The interaction profile of FAME conversion has gotten the curvy shape over the entire range of catalyst dose and methanol to oil molar ratio in contour plot and surface plot of Fig. 9a and b respectively. The reason regarding the aforementioned trends in FAME conversion is already discussed in the OVAT section. The similar trend is also observed in the case of catalyst dose and reaction temperature interaction in Fig. 9c and d. There is a significant increment in FAME conversion from 35 °C to 65 °C as observed in experiments (4,5) at each value of catalyst dose, and; further followed by a drastic decrement as in experiment 6. Fig. 10a and b show the interaction between catalyst dose and reaction time. Here, again, reaction time becomes a limiting factor to some instant; FAME conversion reaches its maxima at each value of catalyst dose. After that, it almost becomes stagnant with feeble loss in ester conversion. The possible interaction between methanol to oil molar ratio and reaction temperature is represented by contour plot and surface plot in Fig. 10c and d accordingly. As methanol to oil molar ratio has a wide range, FAME conversion has got raised till higher ratio at moderate temperatures. Reaction temperature has again followed the same pattern as above said. Fig. 11a and b depicted the parallel interaction of methanol to oil molar ratio and reaction time where both factors behaved synergistically. At last Fig. 11c and d showed the combined effect of reaction temperature and reaction time together. Here, reaction temperature seemed to be the dominating factor over reaction time as in experiments (7, 8, 12, and 13).

*3.3.2.3. Optimization and validation of BBD model in RSM study.* RSM predicted highest FAME conversion at following optimum conditions: catalyst dose; 1.19 wt%, methanol to oil molar ratio; 21.5:1, reaction temperature; 71 °C and reaction time; 97.7 min in Fig. 12. Confirmatory experiments were executed at the optimum condition with little modification in the aforementioned process conditions. Finally, 98% methyl ester conversion was achieved using 1.2 wt% catalyst dose with 22:1 methanol to oil molar ratio at 65 °C in 100 min. This real-time process conditions are almost similar as anticipated by RSM rather than OVAT with a slight deviation in reaction temperature. The selected experimental conditions with their acceptable percentage errors are enlisted in Table S7 (See supplementary). Hence the outcomes from BBD are substantiated the validity of BBD model used in present study. The slight discrepancy in reaction temperature was attributable to a limitation as beyond the boiling temperature of methanol, ester conversion started deteriorating as already discussed in OVAT section.

### *3.3.3. Comparative study of OVAT and RSM*

The process variables such as catalyst dose, methanol to oil molar

**Table 1**
Comparative study of various homogeneous and heterogeneous catalysts employed in biodiesel production from mahua oil.

| Catalysts | Methods | Reaction conditions | | | | Methanol to oil molar ratio | Reaction temperature |
|---|---|---|---|---|---|---|---|
| | | Catalyst amount | | | | | |
| Mn doped ZnO (Heterogeneous) | Transesterification (Magnetic stirring) | 8 wt% | 9:1 | 50 °C | 50 min | Y = 97.0% | (Baskara et al.,2017) [79] |
| KOH (Homogeneous) | Transesterification preceded by acid esterification (Mechanical stirring) | 1.5 wt% | 0.32(v/v)% | 60 °C | 1.5 h | Y = 88.0% | (Muthukumaran et al.,2017) [10] |
| Red mud | Transesterification | 15 g/L of oil | 20v/v% | 60 °C | 0.5 h | Y = 80.0% | (Senthil et al.,2016) [80] |
| Ba-La mixed oxide | Transesterification preceded by acid esterification (Mechanical stirring) | 1.5 wt% | 18:1 | 65 °C | 2 h | C = 97.5% | (Sahani et al.,2018) [5] |
| NaOH (Homogeneous) | Transesterification preceded by acid esterification (Mechanical stirring) | 1 wt% | – | 60 °C | 2 h | – | (puhan et al.,2005) [11] |
| KOH (Homogeneous) | Transesterification preceded by acid esterification (Mechanical stirring) | 0.7w/v% | 0.25v/v | 60 °C | 0.5 h | C = 98.0 ± 0.5% | (Ghadge et al.,2005) [81] |
| KOH (Homogeneous) | Transesterification preceded by acid esterification (Mechanical stirring) | 0.7w/v% | 0.25v/v% | 60 °C | 1 h | – | (Kumar et al.,2017) [82] |
| KOH (Homogeneous) | Microwave assisted two steps Transesterification preceded by acid esterification | 1 wt% | 40 wt% | 53 °C | 2 min | C = 96.0% | (Jothi et al,2013) [83] |
| Sodium methoxide (Homogeneous) | Transesterification preceded by acid esterification (Mechanical stirring) | 8 wt% | 0.33v/v% | 65 °C | 1 h 150% v/v excess alcohol – | C = 95.0% | (Padhi et al.,2010) [84] |
| ZnO (Heterogeneous) | Transesterification | 20 wt% | 40:1 (supercritical Methanol) | 250 °C | 62 min | C = 99.0% | (lamba et al.,2019) [85] |
| $SrTiO_3$ | Transesterification preceded by acid esterification (Mechanical stirring) | 1.2 wt% | 22:1 | 65 °C | 100 min | C = 98.0% | Present study |

ratio, reaction temperature and reaction time have shown their crucial impact on transesterification according to both optimization techniques (OVAT and RSM). But their interactive effects are only shown by RSM which is not possible in the OVAT method. Moreover, the strength of the individual parameter can only be achieved by RSM technique. Apart from this, OVAT for the present study was not sufficient to obtain the FAME conversion more than 90% while RSM was quite successful to scale the FAME conversion up to 98% authenticated by confirmatory experiments in Table S7 (See supplementary) and ascertained the potential of perovskite $SrTiO_3$ as a heterogeneous catalyst for methyl ester production. Furthermore, the catalytic potential of prepared $SrTiO_3$ was compared with previous observations of homogeneous and heterogeneous acid or base catalyst for biodiesel production from mahua oil. Ultimately, perovskite $SrTiO_3$ was observed more efficient for heterogeneous catalysis in transesterification using mild reaction conditions of process variables as illustrated in Table 1.

### 3.4. Kinetic and thermodynamic investigation

Eq. (13) was employed to plot first order kinetic profile of -ln (1-ME) versus t (Fig. 13a). The kinetic plot in Fig. 13a exhibits the rational linearity anticipating the precision of the applied kinetic model of pseudo first order kinetics [61]. Furthermore, the rate constants at temperatures 308 K, 318 K, 328 K and 338 K were determined to be $2.17 \times 10^{-3}$ $min^{-1}$, $3.8 \times 10^{-3}$ $min^{-1}$, $1.0 \times 10^{-2}$ $min^{-1}$ and $1.85 \times 10^{-2}$ $min^{-1}$ respectively. The experimentally derived rate constants support the outcomes that higher temperature accelerates transesterification process owing to promoted mass transfer. The activation energy ($E_a$) and pre-frequency factor (A) are calculated to be 65.983 KJ/mole and $17.8 \times 10^7$ [62] using Arrhenius plot in Fig. 13b. This observed value of activation energy derived on the basis of kinetic experiments found in close agreement with previous reports in literature regarding biodiesel production using heterogeneous catalyst [10,63]. It further interpreted the chemical reaction occurring on the surface of catalyst as the rate determining step also validating the adopted kinetic model in current study. The investigation of thermodynamic functions in transesterification process was helpful in interpreting the mechanism involved in the process. Hence, from Eq. (18) the value of $\Delta H^\circ$ and $\Delta S^\circ$ could be computed from the slope and intercept of the plot ln(k/T) versus 1/T respectively. Fig. 13c depicted the Eyring-Polanyi profile for strontium titanate catalyzed transesterification reaction of mahua oil. The thermodynamic functions ($\Delta H^\circ$ and $\Delta S^\circ$) were evaluated as 63.21 kJ/mol and −291.19 J/mol respectively. The positive $\Delta H^\circ$ value approved the transesterification reaction as endothermic in nature which further justified that external heat energy was critically needed to promote the reactants subsequent transformation into an activated complex [55]. The $\Delta S^\circ$ value found to be negative which possibly attributed to the rapid formation of reactant-catalyst complex that consequently reduced the randomness of the system. From Eq. (12), the $\Delta G^\circ$ values were estimated to be 152.83 kJ/mol, 155.74 kJ/mol, 158.65 kJ/mol and 161.56 kJ/mol for the reaction temperature 35 °C, 45 °C, 55 °C and 65 °C respectively. The positive $\Delta G^\circ$ value indicates the non-spontaneous nature of the reaction in which transition state is having the higher energy level than reactants. Cumulatively, the positive values of $\Delta G^\circ$ and $\Delta H^\circ$ and negative value of $\Delta S^\circ$ indicated the non-spontaneous and endergonic nature of the transesterification reaction [61].

### 3.5. Endurance test

The endurance power of a catalyst during transesterification ensures its sustainability for its economical application. Here, the relative strength of bonds in catalyst owed to the compact structure of perovskite lattice which did not allow the active site to leach into mother liquor. The reusability test ascertained that catalyst was quite efficient for biodiesel production till the sixth cycle ending up to 79% FAME

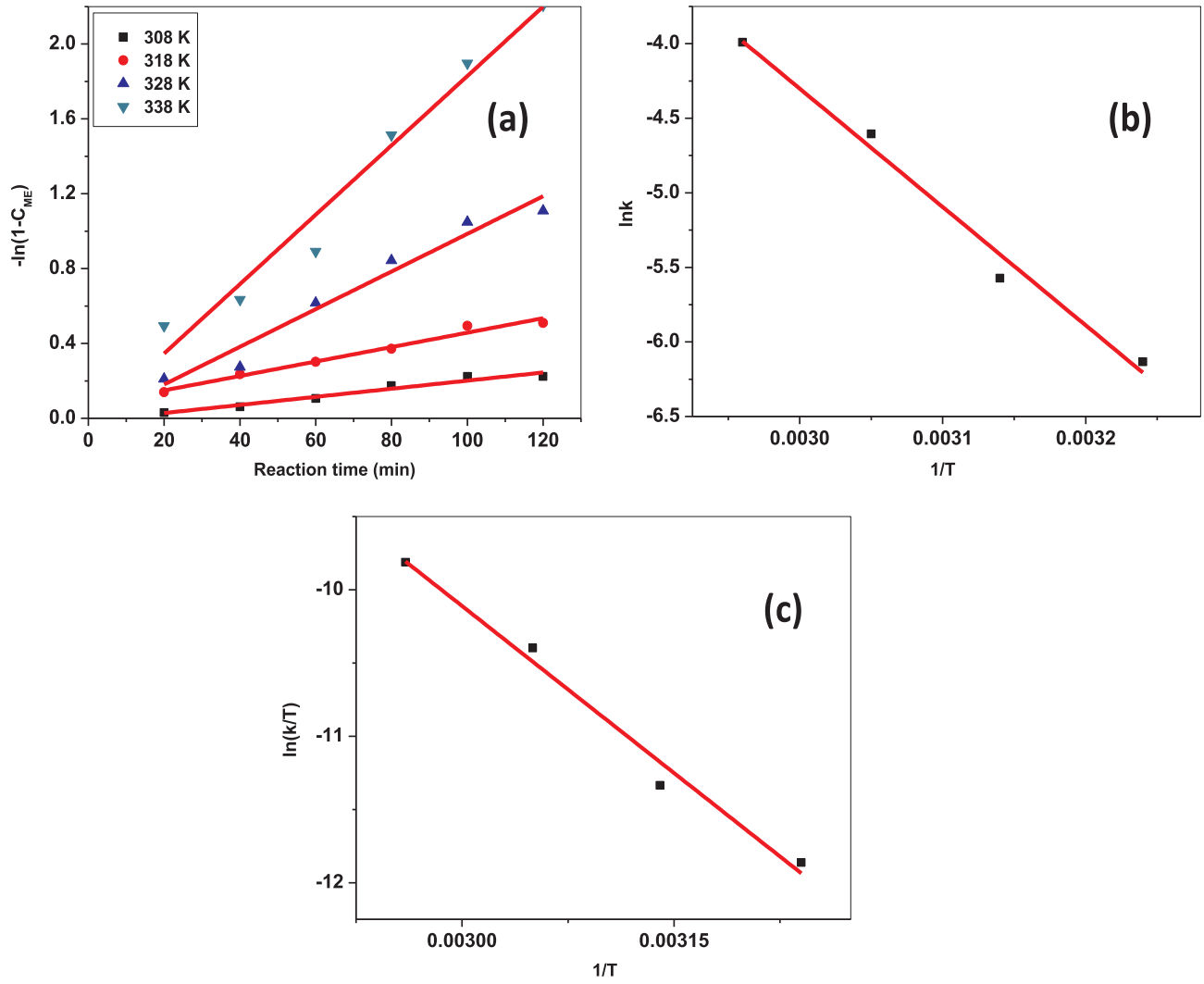


**Fig. 13.** (a) −ln(1 − ME) versus reaction time (min) plot for Pseudo-first order kinetics,(b) Arrhenius plot, (c) Eyring plot.

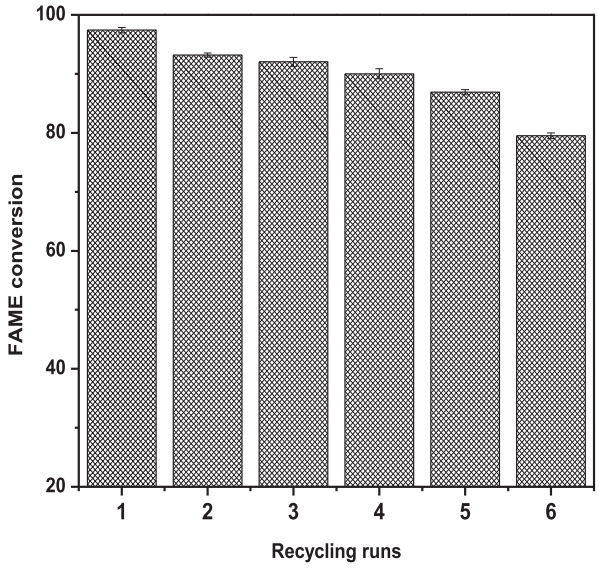


**Fig. 14.** Reusability test of perovskite catalyst.

conversion as in Fig. 14. But soon after, there is a considerable drop in catalyst activity which might be due to blockage or deformation of active site predominantly [48]. Olutoye et al. (2014) [62] explored the three possible reasons for the catalytic deactivation; (*i*) blockage of active sites through irreversible deposition of bulkier molecules[64]; (*ii*) leaching of active species into reaction system in subsequent recycling;(*iii*) loss of catalyst during regeneration process [53]. Fig. S1 (See supplementary) demonstrates the FTIR spectra of spent catalyst before and after regeneration. It manifests the attachment of residues of triglyceride, glycerol and methanol during methanolysis process due to the appearance of high intensity peaks corresponding to ester group and –O-$CH_2$ also depicted in the schematic mechanism later. The results obtained from FTIR of spent catalyst withdrew the conclusion that triglyceride and methanol both molecule firstly get adsorbed onto the surface of catalyst and further proceed for chemical reaction forming FAME [64].

Nevertheless, a plausible mechanism was proposed to comprehend the chemical activity occurring in transesterification process shown in schematic representation (Fig. 15). The entire process of transesterification happened in four steps as schematically drawn in Fig. 15. In step I, both triglyceride and methanol diffused and got adsorbed on the two neighboring active sites following the Langmuir Hinshelwood dual site mechanism [64–66]. Thereafter, methanolysis is executed via nucleophilic attack of methoxide ion resulting diglyceride and methyl ester. Later on, this process is extended to diglyceride and

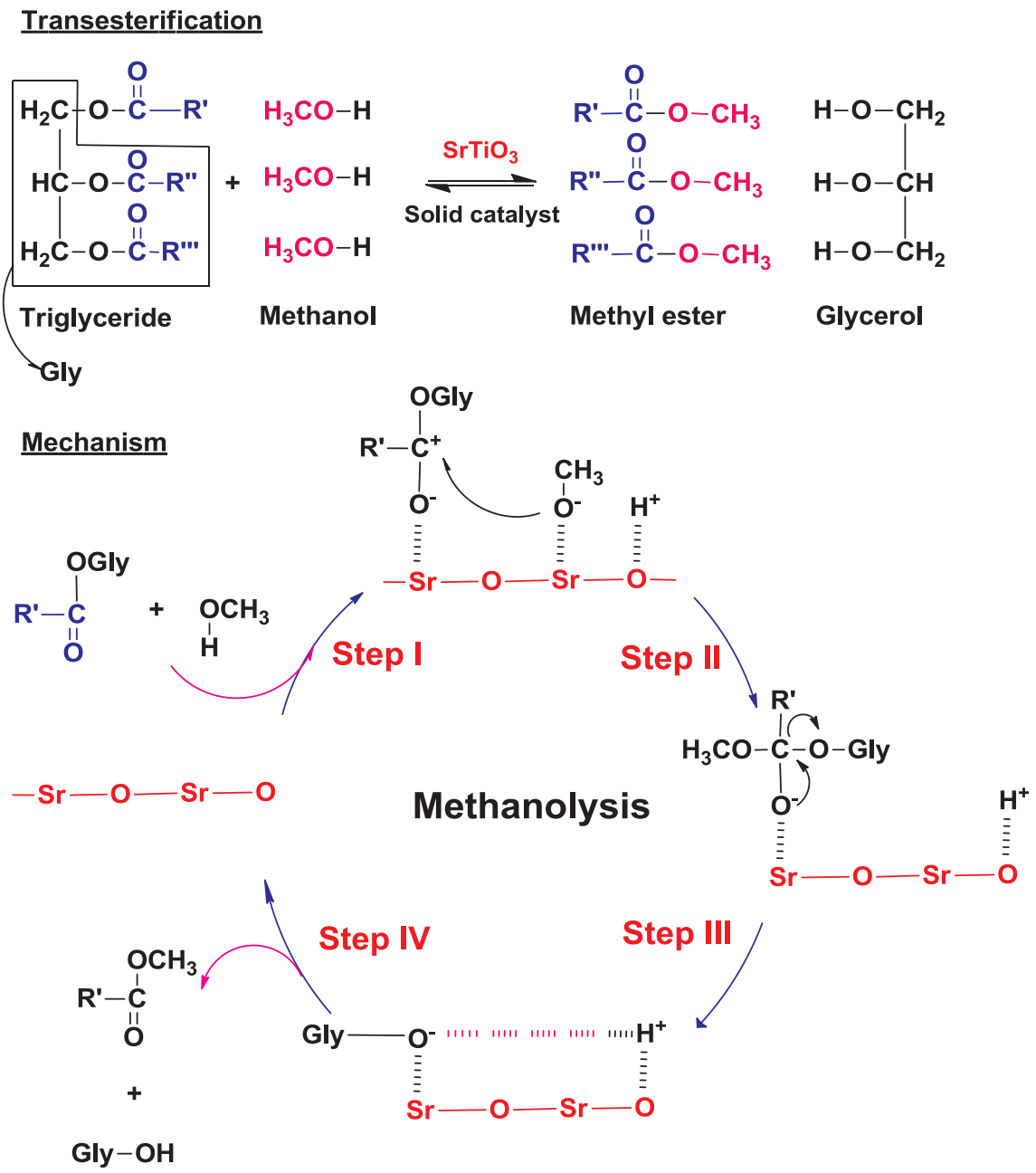


**Fig. 15.** Schematic diagram demonstrating the plausible mechanism of transesterification reaction on the surface of the catalyst.

monoglyceride [65].

### 3.6. Green parameters

The environmental impact of present biodiesel synthesis using transesterification was quantitatively assessed by 'Environmental Factor'. In general, E-factor is defined as "*the mass ratio of waste to the desired product.*" The green approach of this transesterification was estimated by E- factor using the following formula [67].

$$E - Factor = \frac{weightofwaste}{weightofproduct} \quad (20)$$

This calculated to be 0.0926 which indicated transesterification reaction to be a green approach for biodiesel production. This considerably low value of E-Factor manifested a clear insight into the greenness of transesterification reaction for biodiesel production [67]. The turnover frequency (TOF) quantifies the specific catalytic activity of active centre undergoing certain reaction under some defined conditions. It is explicated as number of molecular reactions occurring at the active centre per unit time specifically in solid catalysis. This value is determined using the given formula below.

$$TOF = \frac{Numberofmolesofsubstratesreacted}{Numberofmolesofbasicsitesofcatalyst \times time} \quad (21)$$

Here, TOF for transesterification was calculated to be $23 \times 10^{-2}\ s^{-1}$. This value was observed to be higher enough than TOF values reported in the literature for various catalytic applications [68–71]. In addition to above, the catalytic activity of Sr-Ti based catalysts with different Sr/Ti molar ratio was also analyzed in transesterification reaction detailed in Table S8 (Supplementary Information). Reactions were performed at optimized conditions of process variables mentioned by RSM. The catalyst samples with Sr/Ti stoichiometric ratios of 1:1 and 2:1 were observed to give almost similar FAME conversion. This might be due to the availability of active phase i.e. Sr-O present in catalyst. The catalyst

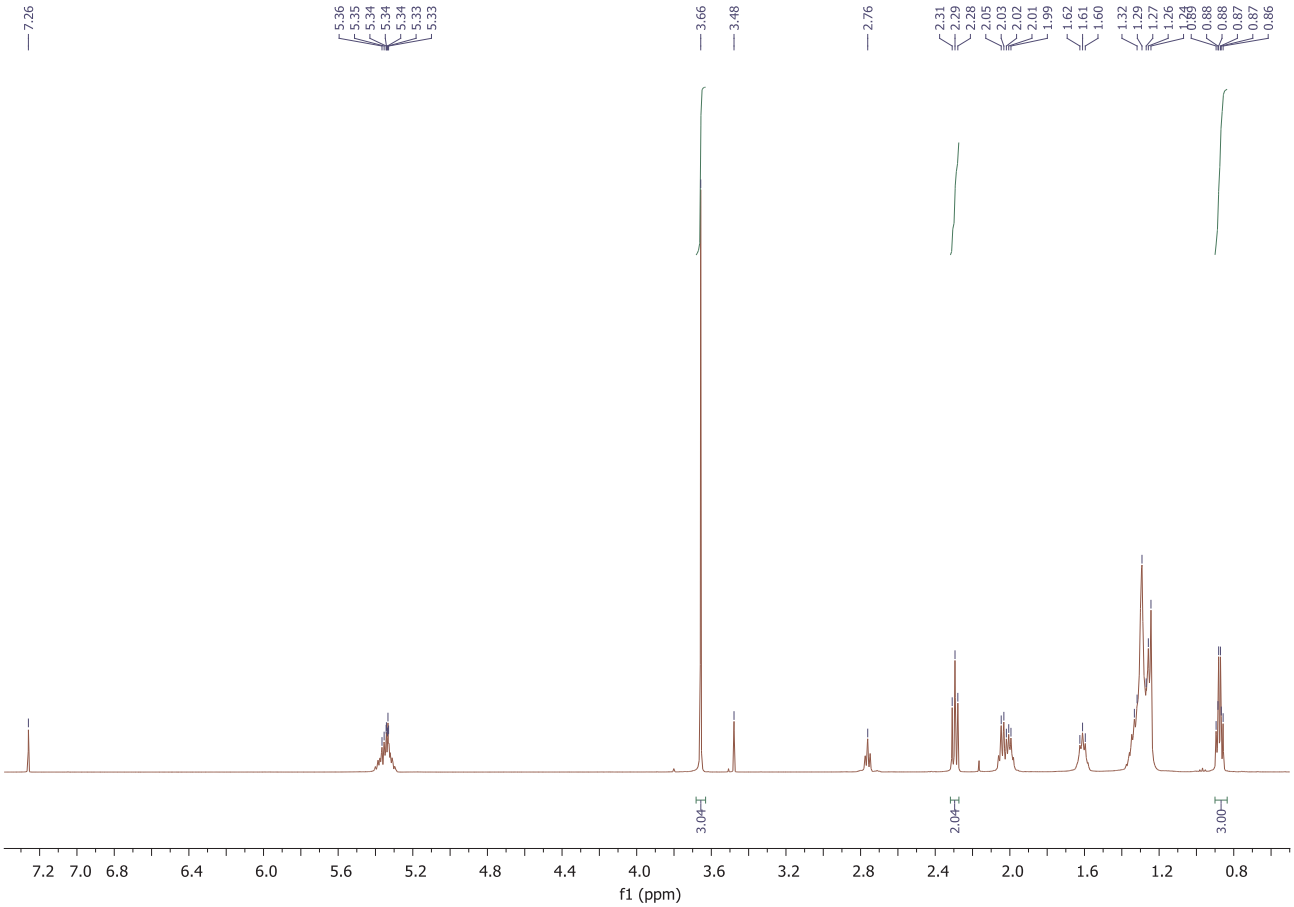


**Fig. 16.** $^{1}$H-NMR spectra of biodiesel produced at optimized conditions of all process parameters (catalyst dose: 1.2 wt%; methanol to oil molar ratio: 22:1; reaction temperature: 65 °C; reaction time: 100 min; agitation speed: 600 rpm).

sample with Sr/Ti (2:1), contains the active sites more than Sr/Ti (1:1). But in this case Sr/Ti (2:1) non stoichiometric Sr except $SrTiO_3$, forms its native oxide which is not stable and undergo for leaching phenomenon which limits its application as a potential and sustainable catalyst while Sr/Ti(1:1) consists of perovskite structure making the catalyst quite sustainable. Here in present study, sustainable catalyst is explored for transesterification. Hence perovskite $SrTiO_3$ is employed for methanolysis and further optimization process was executed for highest FAME conversion. Regarding Sr/Ti (1:2), here, non stoichiometric Ti forms its own native oxide which is not found an active phase for methanolysis reaction rather it only acts as a sustainable support. This might be the reason for its relative lower catalytic activity.

### 3.7. Biodiesel characterization

The synthesized FAME was characterized by FTIR and $^{1}$H NMR. Nonetheless physicochemical and fuel properties were also determined to check the quality of synthesized biodiesel.

#### 3.7.1. $^{1}$H NM

The mahua oil biodiesel was analyzed by $^{1}$H NMR spectroscopy shown in Fig. 16. The characteristic signal attributed to methoxy protons in FAME appeared as a singlet at $\delta$3.66 ppm. The triplet signal at $\delta$ 2.30 ppm was related of α-$CH_2$ protons of ester [72]. The integration values of these two distinct peaks were used to estimate the FAME conversion in Eq. (5). Moreover, triplet signal of the bis-allylic protons (-C = C-$CH_2$-C = C-) present in linoleic acid appeared at $\delta$ 2.76 ppm. The α-CH2 to carbon double bond positioned as multiplet around $\delta$ 2.00–2.05 ppm. A multiplet at $\delta$ 1.59–1.63 ppm displayed the presence of β-methylene protons in methyl ester. The high intensity signals at $\delta$ 1.24 and $\delta$ 1.30 ppm exhibited the backbone methylene protons of fatty acid moiety. The terminal methyl protons of carbon chain in fatty acid were observed as multiplet at $\delta$ 0.85–0.88 ppm. Additionally, a multiplet signal at $\delta$ 5.28 ppm was attributable to olefinic hydrogen present in FAME, respectively [73,74].

#### 3.7.2. $^{13}$C NMR

Fig. 17 illustrated the $^{13}$C NMR spectrum of the mahua oil biodiesel. The signal of carbonyl carbon of methyl ester (-COOMe) in biodiesel emerged at 174.58 ppm while methoxy carbon in FAME appeared at 51.69 ppm. The high intensity signals at128.14–130.45 ppm confirmed the unsaturation due to linoleic acid methyl esters present in biodiesel corroborating the inference from GC–MS [72]. The number of signals at 14 ppm and 22–34 ppm appeared because of carbons of terminal methyl groups and methylene group of long carbon chain in FAME [74].

#### 3.7.3. FTIR

The FTIR spectrum of biodiesel in Fig. 18 conveyed the presence of various functionalities in FAME, which confirmed the absence of phosphorus, sulfur and poly-aromatic groups [75]. Basically, methyl ester is characterized by the high intensity peak near 1740 $cm^{-1}$ owing to C = O stretching frequency. The position of carbonyl band in FTIR spectra is quite sensitive to its adjacent functional groups [72]. In Fig. 18, it was seen that the carbonyl stretching peak was transitioned from 1748 $cm^{-1}$ in mahua oil to 1740 $cm^{-1}$ in FAME [75]. The sharp peak at 3007 $cm^{-1}$ was regarded to olefinic C–H stretching (–HC = CH–) in FAME [75] while the peak appeared at 2922 $cm^{-1}$ owed to asymmetric $CH_3$ stretching and peak observed at 2852 $cm^{-1}$ was attributable to –CH– stretching in O-$CH_3$ [76]. The asymmetric and symmetric vibrations corresponding to $CH_3$ deformation were noticed

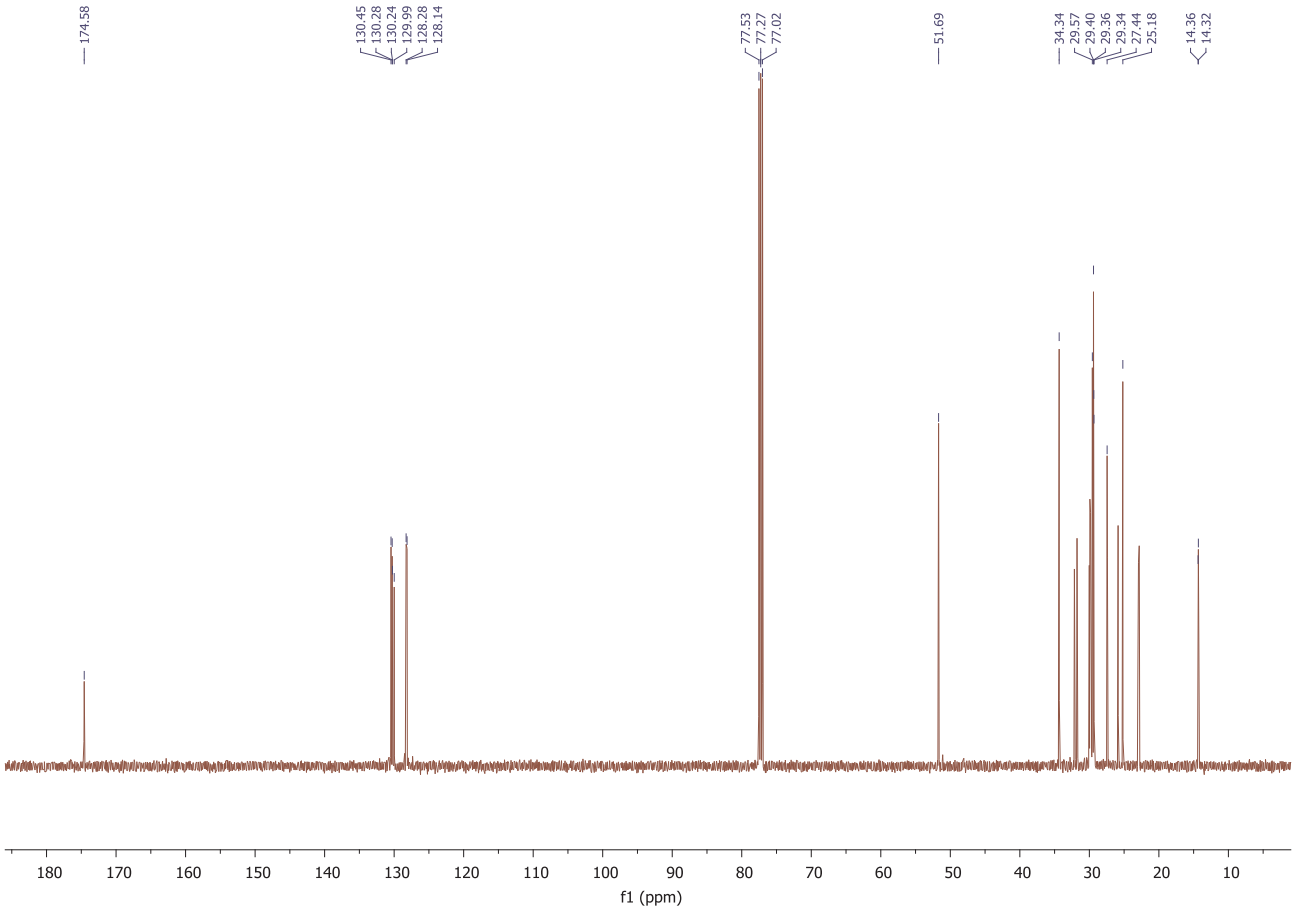


**Fig. 17.** $^{13}$C-NMR spectra of biodiesel produced at optimized conditions of all process parameters (catalyst dose: 1.2 wt%; methanol to oil molar ratio: 22:1; reaction temperature: 65 °C; reaction time: 100 min; agitation speed: 600 rpm).

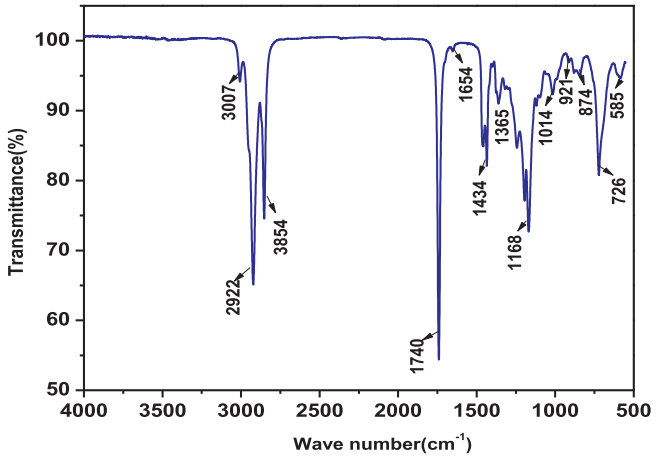


**Fig. 18.** FTIR spectra of mahua oil biodiesel prepared at optimum condition of process variables.

near 1434 cm$^{-1}$ and 1365 cm$^{-1}$ respectively. The low intensity peak at 1654 was assigned to stretching of -C = C- present in the fatty acid moiety. The noticeable peaks at 874 cm$^{-1}$and 585 cm$^{-1}$ were related to -C-O-C- stretching and bending vibrations [72,75]. The peak at 726 cm$^{-1}$ corresponded to $CH_2$ bending vibrations whereas the peak at 921 cm$^{-1}$ presented C–H bending vibration from substituted -C = C- part. Moreover the strong and broad peaks in the range of 1000 cm$^{-1}$ to 1200 cm$^{-1}$ showed the stretching of acyl (-C = O). Ultimately, this typical FTIR spectrum of transesterified mahua oil vindicated the presence of FAME.

### *3.7.4. Physicochemical and fuel properties of methyl ester*

The important physicochemical and fuel properties of synthesized biodiesel from mahua oil were evaluated and found within the permissible limit prescribed by American (D 6751) and European (EN14214) standards for biodiesel [76–78], summarized in Table 2. The density of biodiesel at 40 °C was determined as 0.853gcm$^{-3}$ which was comparable to petrodiesel. The determined value of the specific gravity of biodiesel in the present analysis was comparable to petrodiesel (Table 2). Fluid resistivity or viscosity plays major role by affecting the fuel injection in engines, exclusively at low temperature [76]. The viscosity of biodiesel found was 5.2 cp within the permissible range of ASTM D6751 standard but found a little higher than permissible limit given by EN14214. The pour point of a fuel is the temperature at which the fuel start flowing whereas cloud point is the temperature at which wax are seen first when the fuel is cooled. The pour point and cloud point of mahua oil biodiesel were found in range of −15 °C and 3 °C [72,76] in Table 2 which were noticed to be comparatively low than that of conventional diesel. This made the produced biodiesel comparatively suitable for cold weathers. The flash point and fire point are very critical parameters which are seriously taken into account in the handling, storage and safety of fuels. The observed flash point and fire point of mahua oil are within the limits of ASTM and EN standards (Table 2), in fact, higher than that of petrodiesel ensuring less chance of flammability hazard [33]. This indicates that the produced biodiesel is safer than the petroleum fuel.

## 4. Conclusions

Strontium titanate, a nanocatalyst for transesterification was synthesized by polymer precursor method. The calcination temperature

**Table 2**
Physicochemical and fuel properties of biodiesel produced from mahua oil with ASTM standards.

| Properties | Unit | Feedstock | Biodiesel | Petro Diesel | Biodiesel standards | | | |
|---|---|---|---|---|---|---|---|---|
| | | | | ASTM D0975 | ASTM D 6751 Test methods limit | | DIN EN 14214 Test methods limit | |
| Acid value | mg KOH/g | 14 | 0.49 | 0.35 | D664 | < 0.50 | EN 14104 | < 0.50 |
| Color | – | Yellowish Red | Yellow | Pale yellow | – | – | – | – |
| Calorific value | (MJ/kg) | 38.98 | 36.30 | 44.21 | D4809 | – | – | – |
| Copper strip corrosion | – | 1a | 1a | – | D130 | 3 max | ENISO2160 | 1 |
| Cetane number | – | 38 | 54 | 49 | D 613 | 47 min | EN15195 | 51 min |
| Cloud point | °C | – | −1 | −15 to 5 | D2500 | −3 to 12 | EN23015 | – |
| Density (at R.T.) | g/cm$^3$ | 0.872 | 0.853 | 0.850 | D1298 | 0.875–0.900 | ENISO12185 | 0.860–0.900 |
| Flash point | °C | 210 | 141 | 60–80 | D93 | 130 min | ENISO3679 | 101 min |
| Fire point | °C | 259 | 163 | – | D93 | – | – | – |
| Kinematic Viscosity (at 40 °C) | mm$^2$/s | 24.1 | 5.2 | 1.9–4.1 | D445 | 1.9–6.0 | ENISO3104 | 3.5–5.0 |
| Pour point | °C | – | −4 | −35 to −15 | D97 | −15 to 16 | – | |
| Saponification value | mg KOH/g | 168 | 147 | – | D5558 | 370 max | – | – |

was optimized in order to obtain the most active perovskite phase of the prepared catalyst. Powder XRD, XPS, FESEM, EDX, FTIR and TEM confirmed the perovskite structure of the catalyst with the structural formula of $SrTiO_3$ consisting well-assorted particles in the nano-range. The surface area and basic characteristics of perovskite with $S_{BET}$ (39 m$^2$/g), pore size (7.6 nm), and total basicity (1.89 mmol/g) showed that prepared catalyst has got sufficient basic sites and enough surface exposure for heterogeneous catalysis. Strontium titanate was successfully applied as a heterogeneous base catalyst for transesterification of mahua oil with high FFA content preceded by the esterification reaction. The optimization process of all important reaction parameters was performed via OVAT and RSM using BBD. The following process conditions were pointed out by OVAT: catalyst dose (1.3 wt%), methanol to oil molar ratio (18:1), reaction temperature (65 °C), reaction time (120 min), and agitation speed (600 rpm). Since the initial transesterification reaction predicted agitation speed as an ineffective parameter, this parameter was not taken into account in RSM. The parameters namely catalyst dose (0.3–1.8 wt%), methanol to oil molar ratio (3–23), reaction temperature (35–85 °C), and reaction time (20–120 min) were optimized by BBD. However, RSM attained highest methyl ester conversion at optimum catalyst dose; 1.19 wt%, methanol to oil molar ratio;21.5:1, reaction temperature; 71 °C and reaction time;97.7 min. Confirmatory experiments resulted in the highest 97.9% FAME conversion at following reaction conditions catalyst dose (1.2 wt%), methanol to oil molar ratio (22:1), reaction temperature (65 °C), reaction time (100 min). It depicts the close agreement with predicted values of RSM using BBD rather OVAT. Hence the BBD is one of the suitable designs of experiment to explore the optimum conditions for biodiesel production with a minimum number of experiments. According to RSM, catalyst dose, reaction temperature, reaction time, and methanol to oil molar ratio were most mechanism controlling parameters for transesterification in descending order. Furthermore, a pseudo-first-order model was established with the activation energy ($E_a$) of 65.95kJmol$^{-1}$. Thermodynamic quantities ($\Delta H^\circ$, $\Delta S^\circ$, and $\Delta G^\circ$) were also evaluated to be 63.21kJmol$^{-1}$,-291.19 kJ mol$^{-1}$, and 161.56 kJ mol$^{-1}$ respectively. The positive value of Gibbs free energy ($\Delta G^\circ$) suggested the transesterification reaction as non-spontaneous or external force driven reaction which validates the need of heterogeneous catalysis. The E-factor and turn over frequency (TOF) were also determined and found to be 0.0926 and $23 \times 10^{-2}$ s$^{-1}$. The physicochemical properties of produced biodiesel were found within the permissible limit prescribed by American and European standards for biodiesel (ASTM D-6751 and JUS EN14214) and approved its compatibility with conventional diesel fuel.

## Declaration of Competing Interest

The authors declare that they have no known competing financial interests or personal relationships that could have appeared to influence the work reported in this paper.

## Acknowledgement

Authors acknowledge the support of Central Instrument Facilities, Indian Institute of Technology (BHU), Varanasi India. Authors would also show their great sense of gratitude towards UGC, Delhi, and MHRD, Delhi, for financial assistantship as SRF to SS and TR respectively.

## Appendix A. Supplementary data

Supplementary data to this article can be found online at https://doi.org/10.1016/j.enconman.2019.112180.

## References

[1] Gerpen JV. Biodiesel processing and production. Fuel Process Technol 2005;86(10):1097–107.
[2] Sharma YC, Singh B. Development of biodiesel: current scenario. Renew Sustain Energy Rev 2009;13:1646–51.
[3] Demirbas A. Biodegradability of Biodiesel and Petrodiesel Fuels. Energy Sources Part A Recovery Utilization Environ Effects 2008;31:169–74.
[4] Madhu D, Arora R, Sahani S, Singh V, Sharma YC. Synthesis of High-Quality Biodiesel Using Feedstock and Catalyst Derived from Fish Wastes. J Agric Food Chem 2017;65:2100–9.
[5] Gebremariam SN, Marchetti JM. Biodiesel production through sulfuric acid catalyzed transesterification of acidic oil: techno economic feasibility of different process alternatives. Energy Convers Manage 2018;174:639–48.
[6] Lam MK, Lee KT, Mohamed AR. Homogeneous, heterogeneous and enzymatic catalysis for transesterification of high free fatty acid oil (waste cooking oil) to biodiesel: a review. Biotechnol Adv 2010;28(4):500–18.
[7] Atadashi IM, Aroua MK, Aziz AA, Sulaiman NM. The effects of catalysts in biodiesel production: a review. J Indust Eng Chem 2013;19(1):14–26.
[8] Furuta S, Matsuhashi H, Arata K. Biodiesel fuel production with solid superacid catalysis in fixed bed reactor under atmospheric pressure. Catal Comm 2004;5(12):721–3.
[9] Muthukumaran C, Praniesh R, Navamani P, Swathi R, Sharmila G, Kumar NM. Process optimization and kinetic modeling of biodiesel production using non-edible Madhuca indica oil. Fuel 2017;195:217–25.
[10] Puhan S, Vedaraman N, Ram BVB, Sankarnarayanan G, Jeychandran K. Mahua oil (Madhuca Indica seed oil) methyl ester as biodiesel-preparation and emission characterstics. Biomass Bioenerg 2005;28:87–93.
[11] Singh V, Hameed BH, Sharma YC. Economically viable production of biodiesel from a rural feedstock from eastern India, *P. pinnata* oil using a recyclable laboratory synthesized heterogeneous catalyst. Energy Convers Manage 2016;122:52–62.
[12] Guerra EM, Gude VG. Transesterification of used vegetable oil catalyzed by barium oxide under simultaneous microwave and ultrasound irradiations. Energy Convers Manage 2014;88:633–40.
[13] Puna JF, Correia MJN, Dias APS, Gomes J, Bordado J. Biodiesel production from waste frying oils over lime catalysts. React Kinet Mech Cat 2013;109:405–15.
[14] Sahani S, Sharma YC. Economically viable production of biodiesel using a novel

heterogeneous catalyst: Kinetic and thermodynamic investigations. Energy Convers Manage 2018;171:969–83.
[15] Maiti S, Chowdhury AR, Das AK. Benzoselenadiazole-based nanoporous Covalent Organic Polymer (COP) as efficient room temperature heterogeneous catalyst for biodiesel production. Microporous Mesoporous Mater 2019;283:39–47.
[16] Lee AF, Bennett JA, Manayil JC, Wilson K. Sustainable biodiesel production via esterification and transesterification. Chem Soc Rev 2014;43:7887–916.
[17] Salamatinia B, Iman H, Abdullah AZ. Alkaline Earth Metal Oxide Catalysts for Biodiesel Production from Palm Oil: Elucidation of Process Behaviors and Modeling Using Response Surface Methodology. Iran J Chem Chem Eng 2013;32:113–26.
[18] Liu X, He H, Wang Y, Zhu S. Transesterification of soybean oil to biodiesel using SrO as a solid base catalyst. Catal Comm 2007;8:1107–11.
[19] Mootabadi H, Salamatinia B, Bhatia S, Abdullah AZ. Ultrasonic-assisted biodiesel production process from palm oil using alkaline earth metal oxides as the heterogeneous catalysts. Fuel 2010;89:1818–25.
[20] Faungnawakij K, Yoosuk B, Namuangruk S, Krasae P, Viriyaempikul N, Puttasawat B. Sr-Mg Mixed Oxides as Biodiesel Production Catalysts. Chem Cat Chem 2012;4:209–16.
[21] Li H, Niu S, Lu C, Li J. Calcium oxide functionalized with strontium as heterogeneous transesterification catalyst for biodiesel production. Fuel 2016;176:63–71.
[22] Lima JRO, Ghani YA, Silva RB, Batista FMC, Bini RA, Varanda LC, et al. Strontium zirconate heterogeneous catalyst for biodiesel production: Synthesis, characterization and catalytic activity evaluation. Appl Catal A Gen 2012;445–446:76–82.
[23] Abreu WC, Moura CVR, Costac JCS, Moura EM. Strontium and Nickel Heterogeneous Catalysts for Biodiesel Production from Macaw Oil. J Braz Chem Soc 2017;28:319–27.
[24] Chen CL, Huang CC, Tran DT, Chang JS. Biodiesel synthesis via heterogeneous catalysis using modified strontium oxides as the catalysts. Bioresour Technol 2017;113:8–13.
[25] Chen SY, Mochizuki T, Abe Y, Toba M, Yoshimura Y. Production of high-quality biodiesel fuels from various vegetable oils over Ti-incorporated SBA-15 mesoporous silica. Catal Comm 2013;41:136–9.
[26] Carlucci C, Degennaro L, Luisi R. Titanium Dioxide as a Catalyst in Biodiesel Production. Catal 2019;9:75–99.
[27] Ibrahim DM, Abu-Ayana YM. Preparation of nano alumina via resin synthesis. Mater Chem Phy 2009;113:579–86.
[28] Hwang J, Rao RR, Giordano L, Katayama Y, Yu Y, Horn YS. Perovskites in catalysis and electrocatalysis. Sci 2017;358:751–6.
[29] Green MA, Ho-Baillie A, Snaith HJ. The emergence of perovskite solar cells. Nat Photonics 2014;8(7):506.
[30] Hbaieb K. Exploring strontium titanate as a reforming catalyst for dodecane. Appl Nanosci 2016;6:847–54.
[31] Liu H, Zhao G, Meng X, Ye J. Doping Ba into strontium titanate for enhanced photocatalytic oxygen evolution over its supported Au-based catalysts. Catal Comm 2017;99:127–30.
[32] Feng LL, Zou X, Zhao J, Zhou LJ, Wang DJ, Zhang X, et al. Nanoporous Sr-rich strontium titanate: a stable and superior photocatalyst for $H_2$ evolution. Chem Comm 2013;49:9788–90.
[33] Guharaja S, Moorthy SD, Hasan ZI, Arun B, Ahamed JI, Azarudheen J. Biodiesel production from Mahua *(Madhuca indica)*. Int J Nano Corr Sci Eng 2016;3(1):34–47.
[34] Gusain D, Dubey S, Upadhyay SN, Weng CH, Sharma YC. Studies on optimization of removal of orange G from aqueous solutions by a novel nano adsorbent nano zirconia. J Indust Eng Chem 2016;33:42–50.
[35] Bezerra MA, Santelli RE, Oliveira EP, Villar LS, Escaleira LA. Response surface methodology (RSM) as a tool for optimization in analytical chemistry. Talanta 2008;76:965–77.
[36] Anupam K, Dutta S, Bhattacharjee C, Datta S. Adsorptive removal of chromium (VI) from aqueous solution over powdered activated carbon: optimization through response surface methodology. Chem Eng J 2011;173:135–43.
[37] Maciel AP, Longo E, Leite ER. Nanostructured tin dioxide: synthesis and growth of nano-crystals and nanoribbons. Quim Nova 2003;26:855–62.
[38] Maciel AP, Leite ER, Longo E, Varela JA. Sol-gel modified method for obtaining alpha-alumina nanocoated with rare earth. Ceram 2005;51:52–7.
[39] Lucena PR, Neto ODP, Santos IMG, Souza AG, Longo E, Varel JA. Synthesis by the polymeric precursor method and characterization of undoped and Sn, Cr and V-doped ZrTiO4. J Alloys Comp 2005;397:255–9.
[40] Vujicic D, Comic D, Zarubica A, Micic R, Boskovi G. Kinetics of biodiesel synthesis from sunflower oil over CaO heterogeneous catalyst. Fuel 2010;89:2054–61.
[41] Yadav M, Singh V, Sharma YC. Methyl transesterification of waste cooking oil using a laboratory synthesized reusable heterogeneous base catalyst: Process optimization and homogeneity study of catalyst. Energy Convers Manage 2017;148:1438–52.
[42] Singh AK, Fernando SD. Reaction kinetics of soybean oil transesterification using heterogeneous metal oxide catalysts. Chem Eng Technol 2007;30:1716–20.
[43] Kaur N, Ali A. Biodiesel production via ethanolysis of jatropha oil using molybdenum impregnated calcium oxide as solid catalyst. RSC Adv 2015;5:13285–95.
[44] Singh B, Bux F, Sharma YC. Comparison of homogeneous and heterogeneous catalysis for synthesis of biodiesel from *Madhuca indica* oil. Chem Indust Chem Eng Quart. 2011;17(2):117–24.
[45] Ghadge SV, Raheman H. Process optimization for biodiesel production from mahua *(Madhuca indica)* oil using response surface methodology. Bioresour Technol 2006;97(3):379–84.
[46] Lakhlifi H, Benchikhi M, Ouatib RE, Er-Rakho L, Guillemet-Fritsch S, Durand B. Synthesis and physicochemical characterization of pigments based on molybdenum « $ZnO$-$MoO_3$: $Co^{2+}$ ». J Mater Environ Sci 2015;6(12):3465–9.
[47] Wang ZB, Yin GP, Shi PF. Effects of ozone treatment of carbon support on Pt–Ru/Ccatalysts performance for direct methanol fuel cell. Carbon 2006;44:133–40.
[48] Yang SF, Niu CG, Huang DW, Zhang H, Liang C, Zing GM. SrTiO3 nanocubes decorated with Ag/AgCl nanoparticles as photocatalysts with enhanced visible-light photocatalytic activity towards the degradation of dyes, phenol and bisphenol A. Environ Sci Nano 2017;4:585–95.
[49] Philleux ME, Grahmann CR, Fuenzalida VM. Hydrothermal strontium titanate films on titanium: An XPS and AES depth profiling study. J Amer Ceramic Soc 1994;77:1601–4.
[50] Shahabuddin S, Sarih NM, Mohamad S, Ching JJ. $SrTiO_3$ Nanocube-Doped Polyaniline Nanocomposites with Enhanced Photocatalytic Degradation of Methylene Blue under Visible Light. Polymers 2016;8:27–42.
[51] Xian T, Yang H, Di L, Ma J, Zhang H, Dai J. Photocatalytic reduction synthesis of $SrTiO_3$-graphene nanocomposites and their enhanced photocatalytic activity. Nanoscale Res Lett 2014;9:327–35.
[52] Last JT. Infrared-absorption studies on barium titanate and related materials. Phy Rev 1957;105:1740–50.
[53] Moura CVR, Neres HLS, Lima MG, Moura EM, Neto JMM, Oliveira JE, et al. Cr/Al Oxide as Solid Acid Catalyst to Afford Babassu Biodisel. J Braz Chem Soc 2016;27:515–25.
[54] Balat M, Balat H. Progress in biodiesel processing. Appl Energy 2010;87:1815–35.
[55] Musa IA. The effects of alcohol to oil molar ratios and the type of alcohol on biodiesel production using transesterification process. Egypt J Petrol 2016;25:21–31.
[56] Fukuda H, Kondo A, Noda H. Biodiesel fuel production by transesterification of oils. J. Biosci. Bioeng. 2001;92:405–16.
[57] Narasimharao K, Lee A, Wilson K. Catalysts in production of biodiesel: a review. J. Biobased Mater Bioenerg 2007;1:19–30.
[58] Mowla D, Rasti N, Keshavarz P. Transesterification of Waste Cooking Oil for Biodiesel Production Using Modified Clinoptilolite Zeolite as a Heterogeneous Catalyst. Int J Chem Molecular Eng 2016;10:1201–6.
[59] Silva WLGD, Souza PTD, Shimamoto GG, Tubino M. Separation of the glyc- erol-biodiesel phases in an ethyl transesterification synthetic route using water. J Braz Chem Soc 2015;26:1743–4.
[60] Mbah GO, Onyiah MI, Amulu NF. Effects of process parameters on biodiesel production from used soy oil. Int J Eng Res Sci Tech 2013;2:46–60.
[61] Nautiyal P, Subramanian KA, Dastidar MG. Kinetic and thermodynamic studies on biodiesel production from *Spirulina platensis* algae biomass using single stage extraction–transesterification process. Fuel 2014;135:228–34.
[62] Olutoye MA, Wong CP, Chin LH, Hameed BH. Synthesis of FAME from the methanolysis of palm fatty acid distillate using highly active solid oxide acid catalyst. Fuel Process Technol 2014;124:54–60.
[63] Mendonca IM, Paes OA, Maia PJ, Souza MP, Almeida RA, Silva CC, et al. New heterogeneous catalyst for biodiesel production from waste tucuma peels (Astrocaryum aculeatum Meyer): parameters optimization study. Renew Energy 2019;130:103–10.
[64] Yan S, Kim M, Salley SO, Ng KYS. Oil transesterification over calcium oxides modified with lanthanum. Appl Catal A Gen 2009;360:163–70.
[65] Endalew AK, Kiros Y, Zanzi R. Inorganic heterogeneous catalysts for biodiesel production from vegetable oils. Biomass Bioenerg 2011;35:3787–809.
[66] Hattori H, Shima M, Kabashima H. Alcoholysis of ester and epoxide catalyzed by solid bases. Stud Surf Sci Catal 2000;130:3507–12.
[67] Guerra EM, Gude VG. Assessment of Sustainability Indicators for Biodiesel Production. Appl Sci 2017;7:869–82.
[68] Kulkarni D, Wachs IE. Isopropanol oxidation by pure metal oxide catalysts: number of active surface sites and turnover frequencies. Appl Catal A Gen 2002;237:121–37.
[69] Ranganathan ES, Bej SK, Thompson LT. Methanol steam reforming over Pd/ZnO and $Pd/CeO_2$ catalysts. Appl Catal A Gen 2005;289:153–62.
[70] Van der Waal JC, Rigutto MS, Van Bekkum H. Zeolite titanium beta as a selective catalyst in the epoxidation of bulky alkenes. Appl Catal A Gen 1998;167(2):331–42.
[71] Bordawekar SV, Doskocil EJ, Davis RJ. Influence of support composition on the structure and reactivity of strontium base catalysts. Catal lett 1997;44(3–4):193–9.
[72] Tariq M, Ali S, Ahmad F, Ahmad M, Zafar M, Khalid N, et al. Identification, FT-IR, NMR ($^1$H and $^{13}$C) and GC/MS studies of fatty acid methyl esters in biodiesel from rocket seed oil. Fuel Process Technol 2011;92:336–41.
[73] Mello VM, Oliveira FCC, Fraga WG, Nascimento CJD, Suarez PAZ. Determination of the content of fatty acid methyl esters (FAME) in biodiesel samples using $^1$H NMR spectroscopy. Magn Reson Chem 2008;46:1051–4.
[74] Monteiro MR, Ambrozin ARP, Liao LM, Ferreira AG. Determination of biodiesel blend levels in different diesel samples by $^1$H NMR. Fuel 2009;88:691–6.
[75] Devi RM, Raj RSSP, Sivakumar M. Comparative Studies on Biodiesel from Rubber Seed Oil Using Homogeneous and Heterogeneous Catalysts. Int J Green Energy 2015;12:1215–21.
[76] Acharya N, Nanda P, Nanda S, Acharya S. Analysis of properties and estimation of optimum blending ratio of blended mahua biodiesel. Eng Sci Tech Int J 2017;20:511–7.
[77] Ambata I, Srivastavaa V, Sillanpaa M. Recent advancement in biodiesel production methodologies using various feedstocks: A review. Renew Sustain Energy Rev 2018;90:356–69.
[78] Patel RL, Sankhavara CD. Biodiesel production from karanja oil and its use in diesel engine: a review. Renew Sustain Energy Rev 2017;71:464–74.
[79] Baskara G, Gurugulladevia A, Nishanthinia T, Aiswaryaa R, Tamilarasan K. Optimization and kinetics of biodiesel production from Mahua oil using manganese doped zinc oxide nanocatalyst. Renew Energy 2017;103:641–6.
[80] Senthil M, Visagavel K, Saravanan CG, Rajendran K. Investigations of red mud as a catalyst in Mahua oil biodiesel production and its engine performance. Fuel Process Technol 2016;149:7–14.
[81] Ghadge SV, Raheman H. Biodiesel production from mahua *(Madhuca indica)* oil

having high free fatty acids. Biomass Bioenerg 2005;28:601–5.
[82] Kumar MV, Babu AV, Kumar PR. Producing biodiesel from crude Mahua oil by two steps of transesterification process. Australian J Mech Eng 2017;17:2–7.
[83] Jothi N, Manivannan A. Optimization of microwave-assisted transesterification of mahua oil using response surface methodology. Int J Sci Eng Technol Res 2013;2:1411–22.
[84] Padhi SK, Singh RK. Optimization of esterification and transesterification of Mahua *(Madhuca Indica)* oil for production of biodiesel. J Chem Pharm Res 2010;2(5):599–608.
[85] Lamba N, Gupta R, Modak JM, Madras G. ZnO catalyzed transesterification of *Madhuca indica* oil in supercritical methanol. Fuel 2019;242:323–33.